J. Fluid Mech. (1998), *vol.* 360, *pp.* 179–211. Printed in the United Kingdom

Active control of streamwise vortices and streaks in boundary layers

By STUART A. JACOBSON† AND WILLIAM C. REYNOLDS

Department of Mechanical Engineering, Stanford University, Stanford, CA 94305, USA

(Received 4 November 1996 and in revised form 18 November 1997)

Coherent structures play an important role in the dynamics of turbulent shear flows. The ability to control coherent structures could have significant technological benefits with respect to flow phenomena such as skin friction drag, transition, mixing, and separation. This paper describes the development of an actuator concept that could be used in large arrays for actively controlling transitional and turbulent boundary layers. The actuator consists of a piezoelectrically driven cantilever mounted flush with the flow wall. When driven, the resulting flow disturbance over the actuator is a quasi-steady pair of counter-rotating streamwise vortices with common-flow away from the wall. The vortices decay rapidly downstream of the actuator; however, they produce a set of high- and low-speed streaks that persist far downstream (well over 40 displacement thicknesses). The amplitude of the actuator drive signal controls the strength of the generated vortices. The actuator is fast, compact, and generates a substantial disturbance in the flow. Its performance has been demonstrated using a small array of sensors and actuators in low-speed water laminar boundary layers with imposed steady and unsteady disturbances. Experiments are reported in which transition from a large disturbance was delayed by 40 displacement thicknesses, and in which the mean and spanwise variation of wall shear under an array of high- and low-speed streaks was substantially reduced downstream of a single transverse array of actuators.

1. Introduction and objectives

Increased understanding of the mechanisms of turbulence has spurred interest in the possibility of turbulence control. The notion that a turbulent flow is dominated by organized coherent structures has led to the idea of trying to control a flow by interacting with these structures. This could provide substantial technological benefits, as well as a new tool for probing the physics of turbulence.

A boundary layer control system is envisioned consisting of a two-dimensional array of actuators, surrounded by sensors whose measurements are used to prescribe the actuator control signal. A sophisticated set of distributed local controllers, based on physical models of the turbulence with real time adaptivity, would coordinate the actuators and the sensors.

The popularity of active turbulence control is reflected in the multiplicity of reviews written on the subject in recent years (Bushnell & McGinley 1989; Fiedler & Fernholz 1990; Moin & Bewley 1994; Gad-el-Hak 1996). Research has focused on means for

† Present address: Department of Aeronautics and Astronautics, MIT, Cambridge, MA 02139, USA.

reducing the drag in a turbulent boundary layer, and on means for delaying the laminar to turbulent transition.

It is generally accepted that there is a relationship between near-wall streamwise vortices and the increase in skin friction observed in turbulent boundary layers. The exact relationship, though, is still an active area of research. The relationship may be direct: Orlandi & Jiménez (1994) claimed that the momentum transported by the streamwise vortices not only generates the streaks, but as a result of the nonlinear nature of the boundary layer, the streaks themselves account for the increase in skin friction observed in turbulent boundary layers. The relationship may instead be indirect: the streaks and streamwise vortices may help contribute to an instability in the flow by the development of an inflectional spanwise or wall-normal profile of the streamwise velocity, leading to a breakdown of the structures and a resulting high skin friction event. Swearingen & Blackwelder (1987) showed that the instability associated with inflectional spanwise profiles of the streamwise velocity, formed by streamwise vortices, was dynamically significant. Results from Acarlar & Smith (1987) suggest that the shear layer instability resulting from the inflectional wall-normal velocity profile associated with low-speed streaks may play a part in the cyclic bursting phenomena. Regardless of the precise relationship, the development of a control system capable of interacting with streamwise wall layer vortices and streaks would be an important step towards the development of a near-wall boundary layer control system.

The scales of the dominant turbulence in the near-wall region provide severe constraints for the actuator and associated control hardware. The average spanwise spacing of the near-wall low-speed streaks is $\Delta z^+ \approx 100$ (Kline *et al.* 1967), and the average streamwise length is $\Delta x^+ \approx 1000$ (Blackwelder & Eckelmann 1978). Here the values are normalized on the wall-unit length scale ν/u_τ, where u_τ is the wall shear velocity and ν is the kinematic viscosity. The wall eddies erupt at an average frequency, normalized by the time scale ν/u_τ^2, of $f_b^+ = 0.004$ (Blackwelder & Haritonidis 1983). A broad distribution of scales is observed, so it is necessary to have control to a fraction of these scales. Hence the spanwise dimension of the control module should be of the order of $20\nu/u_\tau$, and the streamwise dimension about $200\nu/u_\tau$, resulting in a control module area $A_c^+ \approx 4000$. In order to respond quickly enough to a burst, the control electronics have to respond at a rate of about $f_b^+ = 0.02$. Sensors, actuators, and electronics that can meet these challenges do not at present exist.

Because the pacing item for turbulent boundary control seems likely to be actuator development, the present work has concentrated on actuation. The main objectives of this program were to develop an actuator with the potential for active control of transitional and turbulent boundary layers, and to demonstrate control on steady and unsteady streamwise vortex disturbances in a laminar boundary layer, similar to the wall region eddies found in turbulent boundary layers. Experiments were conducted in a low-speed water flow, where the eddy structures are relatively large and slow and hence can be studied under controlled conditions. The work outlined here is described in detail in Jacobson & Reynolds (1995, hereafter denoted by JR).

2. Actuator

2.1. *Concept*

The idea behind the actuator is to modify the near-wall flow by drawing fluid into the wall and pumping it back out in a controlled, directed manner. The JR actuator uses

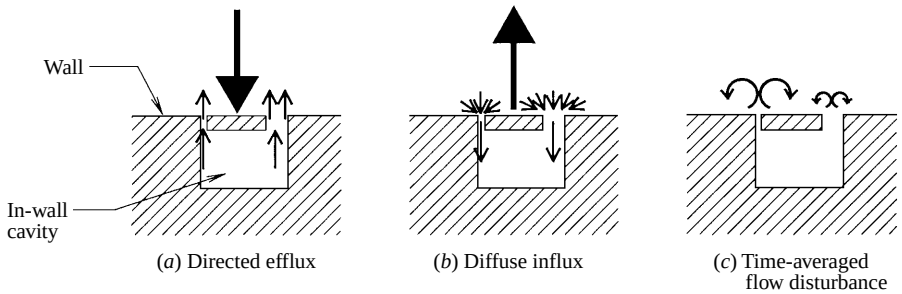

FIGURE 1. Flow disturbance as a cantilevered section of the wall moves into and out of a wall cavity. Flow is forced through the side gaps formed between the moving and stationary wall sections.

surface motion to achieve this objective. A portion of the flow surface is oscillated in and out of a cavity in the surface, resulting in flow patterns shown schematically in figure 1. The fluid influx to the cavity is diffuse, but the efflux is directed, with the result that the primary induced flows are two pairs of counter-rotating vortices, centred over the side gaps, with common flow away from the surface. An important feature is that the side gaps are unequal in width. Observation of the flow disturbance showed a much stronger vortex pair over the narrow side gap than over the wide side gap. Results demonstrating this actuator concept were first presented in Jacobson & Reynolds (1993).

In a two-dimensional numerical simulation, Koumoutsakos (1995) (also Saddoughi *et al.* 1997) identified two types of flow disturbances generated by the actuator concept described in the previous paragraph. Disturbance type I consisted of a quasi-steady vortex pair located over the narrow gap and only a weak disturbance over the wide gap. This disturbance type was generated for the parameters of the actuator described in this paper. Koumoutsakos found that the vortex pair was produced by the downward motion of the oscillating flow surface. The oscillating motion continuously fed the vortices, overcoming diffusion, and the upward motion of the surface balanced out the self-induced velocity of the vortex pair. Disturbance type II consisted of a jet of fluid emerging from the wide gap, with only a weak disturbance located over the narrow gap. The disturbance type for a given actuator configuration depended on flow Reynolds number, geometry, and oscillation frequency.

For the actuator described in this paper, the oscillating surface is a cantilevered section of the boundary surface, with the free end on the downstream side. A piezoelectric material bonded to the underside of the thin stainless steel surface sheeting provides the actuation. The steady deflections that can be achieved with this system are too small to have any effect on the flow, but by operating the cantilever at its resonance frequency a more substantial amplitude can be achieved, and the desired flow patterns can be established.

The idea of using resonant oscillations was introduced for free shear layer control by Wiltse & Glezer (1993), who modulated the forcing amplitude in order to vary the strength of the control. The same procedure was used in the present work. By varying the amplitude of the drive signal, vortices of varying strength can be generated. In this respect, the actuator is a controllable vortex pair generator, with zero net mass flow through the boundary surface.

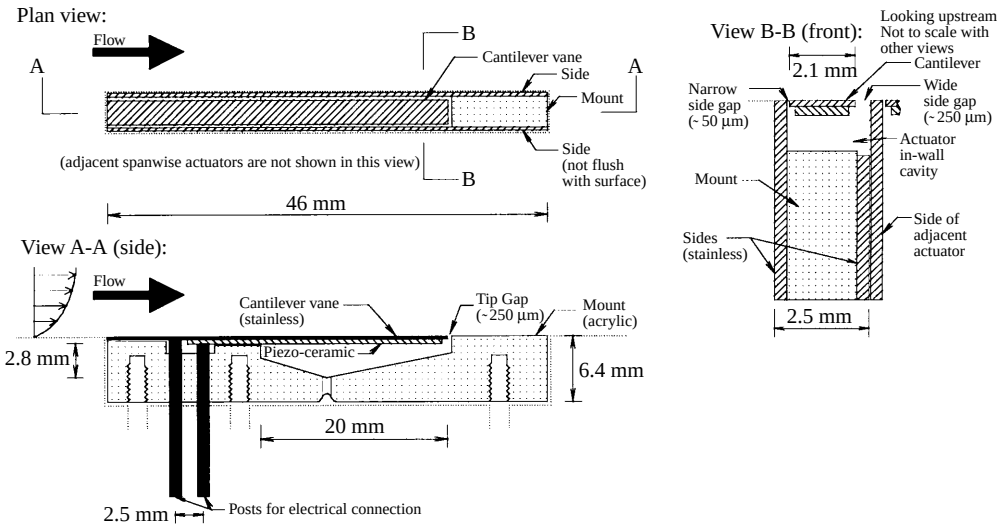

FIGURE 2. Mounted actuator diagram.

2.2. *Design*

The piezoelectric cantilever consisted of a 0.13 mm thick stainless steel vane bonded to a 0.28 mm thick piece of PZT-5H piezo-ceramic. The free length of the cantilever was $L_{act} = 20$ mm, and its width was 2.1 mm. The piezo-ceramic was electrically insulated from the surrounding liquid using a combination epoxy/acrylic coating. When operated submerged in water, the first-mode resonance frequency was approximately 330 Hz.

The cantilever was attached to an acrylic mount that extended both upstream and downstream of the cantilever, and formed the outline for the under-cantilever wall cavity. The mount had three screw holes for attaching the actuator to the test wall, which was the upper wall of the flow channel. A bleed hole was provided so that air could be removed before operation. Figure 2 shows a diagram of a mounted cantilever actuator.

Stainless steel sides were attached to each acrylic mount, isolating the cavity of each actuator from that of an adjacent actuator. One stainless steel side extended to the boundary surface, forming an edge of the narrow side gap, giving tight control of this gap dimension. On the opposite side, the stainless steel side piece was not extended to the surface, and so the wide side gap was formed with the side of an adjacent actuator. The narrow and wide gaps were nominally 50 and 250 μm, respectively, and the tip gap was approximately 250 μm.

The actuator flow disturbance depended strongly on the configuration of the side gaps. The fabrication process allowed at best ± 25 μm control on the narrow side-gap width. This is significant, considering that the narrow side-gap width was a nominal 50 μm. This led to a large variation between the actuators in the magnitude of the actuator flow disturbance for a given drive signal. However, all actuators produced the same qualitative structures as confirmed by flow visualization. All of the actuators used for the results presented here had narrow side-gap widths of approximately 50 ± 10 μm.

The total actuator width was 2.5 mm. This width was chosen based on the relative spacing of standard electrical pin strip headers, which are spaced on a 2.54 mm (0.1 in.)

grid. Hence, the two electrical pins of each cantilever were also spaced 2.5 mm in the streamwise direction. This meant that actuators could be tightly packed in a spanwise array, and the electrical connection made with a standard IDC wiremount socket. The 2.5 mm width dimension was equivalent to 20–70 wall units for the flows obtainable in the tunnel used, putting the actuator width in the desirable range for near-wall boundary layer control.

The actuator was driven with an amplitude-modulated sinusoidal voltage. The signal was first generated at low voltages and then amplified to the voltage range required for the actuator. The resulting signal had a frequency equal to the nominal actuator resonance frequency of 330 Hz, and an amplitude (zero-to-peak) that could be varied from 0 to 25 V. The control computer specified the drive amplitude only. Dedicated circuitry combined the amplitude signal with a sinusoidal voltage to produce the drive signal for each actuator.

The oscillating voltage signal was supplied to the exposed piezo-ceramic surface of the cantilever, which was electrically insulated from the surrounding water. The stainless steel surface was connected to ground and not insulated from the surrounding flow. Applied voltages greater than 25 V caused the insulation around the piezo-ceramic surface to fail, resulting in the formation of small bubbles from electrolysis.

Actuators tested in water showed minimal degradation in the actuator flow disturbance when run for over 100 hours (10^8 cycles). Actuator failures were generally due to mishandling and not to use. Actuators that were fabricated properly, and insulated well from the water, continued working with approximately the same characteristics throughout the project.

2.3. *Actuator flow disturbance*

This section presents measurements of the velocity disturbance caused by a single actuator, along with a visualization of the disturbance. The measurements were taken in a well-controlled steady water flow having a zero-pressure-gradient laminar boundary layer with $U_\infty = 0.24$ m s^{-1} and a displacement thickness (δ^*) = 2.7 mm, corresponding to $Re_{\delta^*} = U_\infty \delta^*/\nu \approx 600$ at the actuator tip (downstream end of the actuator cantilever). The actuator tip was located 51 cm downstream of the boundary layer leading edge ($Re_x \approx 110\,000$). The fly-over time of a fluid particle in the free stream, $t_{f\infty} = L_{\text{act}}/U_\infty$, a useful reference time in the subsequent discussion, is therefore approximately $t_{f\infty} = 0.082$ s. At the oscillation frequency of 330 Hz, there are approximately 30 cycles per $t_{f\infty}$.

The results shown are a compilation taken from several different actuators, and are indicative of their capabilities. As was discussed earlier, slight fabrication differences among the actuators resulted in them producing different strength disturbances for a given drive amplitude. Thus, the actuator amplitude for a given data set is not useful for comparative purposes to other results. Actuator amplitudes are only reported where they are relevant.

2.3.1. *Visualization*

With the actuator operating in a laminar boundary layer and driven at constant amplitude, the flow around the actuator was visualized using fluorescein dye and an argon-ion laser sheet. The dye was introduced upstream of the actuator, along the wall. The laser sheet was formed using a cylindrical lens, and oriented in the (z, y)-plane, where y is the wall-normal direction and z is the spanwise direction. A typical result is shown in figure 3.

A single vortex pair is the dominant feature in the photograph shown in figure 3.

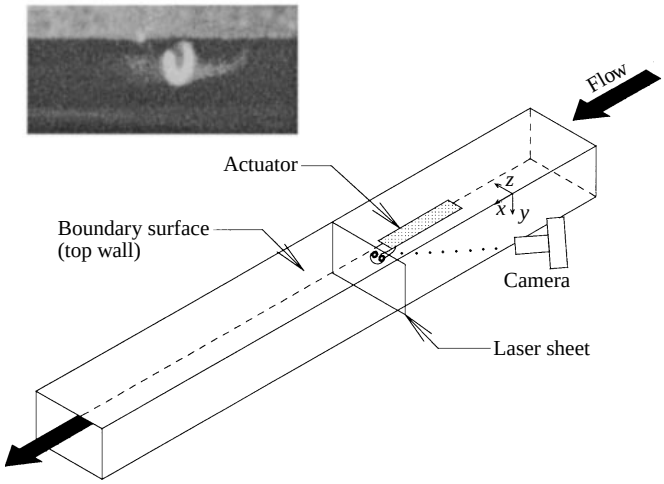

FIGURE 3. Actuator flow disturbance, as visualized using fluorescein dye and a laser sheet. The lighter area on the top portion of the photograph is the wall and the darker area is the flow.

The size and relative location of the vortices will be made clear later using velocity measurements. This vortex pair is the one associated with the narrow side gap. The disturbance over the wide side gap does not appear in the photograph. The wide side-gap disturbance was sometimes visible, but it was much fainter and about an order of magnitude smaller than the narrow side-gap disturbance. The laser sheet had finite depth, and due to the angle at which the photograph was taken, a plume of dye emanating from the wall is faintly visible, at a location upstream of the main visualization plane. This is consistent with velocity measurements, presented later in this section, which show significant normal velocity emanating from the narrow side gap of the actuator.

The vortex pair started about 5 mm upstream of the actuator tip (about 3/4 of the way down the narrow side gap), and grew in size until it reached the actuator tip. For several centimetres downstream of the actuator tip, the dye remained coherent and the structure approximately retained its size. Further downstream, the structure started to lose visual coherence.

We rotated the actuator and then tested it with the cantilever tip located on the upstream end of the actuator. Flow visualization showed similar structures developing as were observed for the downstream facing cantilever. The structure again was visible only towards the downstream end of the cantilever and grew until the downstream end, which in this case was the fixed end of the cantilever. This configuration for the actuator was not pursued further.

These observations indicate that the maximum disturbance is independent of the point of maximum actuator displacement amplitude. Instead, the disturbance appears to occur from an additive effect as it convects downstream and is acted upon repeatedly by the flapping cantilever during the fly-by. This additive concept also explains why no appreciable structure was observed emanating from the actuator tip gap, since the tip gap had no streamwise extent.

2.3.2. *Mean flow*

Velocities were measured using a two-component laser Doppler anemometer (LDA). Results are shown with the wall located at $y = 0$. The velocity signals were analog

low-pass filtered at 90 Hz to remove electronic noise. Data were sampled at 200 Hz and averaged over 1280 measurements. These parameters are valid for all velocity results presented here, except where otherwise noted.

Figure 4 shows contours of the mean velocity disturbance for a relatively strong actuator, operated near maximum amplitude. The data were measured at $\Delta x/\delta^* = 4$, where Δx refers to the distance downstream of the actuator tip. The mean velocity disturbances, ΔU and ΔV, are defined as the difference between the measured velocity of the disturbed flow and the measured velocity of the undisturbed flow. The disturbance can result from the actuator, from streamwise vortices introduced upstream of the actuator, or from the interaction of the two. In this section, the disturbance results from the actuator alone. Positive contours are shown as solid lines and negative contours as dotted lines. Positive V indicates flow away from the wall.

The contours were generated from a grid of data, spaced uniformly in the spanwise direction and non-uniformly in the wall-normal direction, with a denser spacing near the wall. The grid points are indicated by dots in figure 4(*a*). For generating the near-wall contours, the data were extended to the wall by assuming zero velocity at the wall.

The LDA measuring volume was precisely located to confirm that the maximum V disturbance was aligned with the narrow side gap of the actuator. The wide side gap is located in figure 4 at $z/\delta^* \approx 0.9$. No disturbance was measurable over the wide side gap at this streamwise location. (The LDA had a resolution of $\Delta U/U_\infty \approx \Delta V/U_\infty \approx 0.002$.) For the runs presented here, the zero for the spanwise traverse was set to the location of the maximum measured V, which was considered equivalent to aligning with the narrow side gap of the actuator, but was a simpler alignment to perform.

The V disturbance in figure 4 shows a strong concentrated velocity away from the wall, with maximum velocity located about δ^* from the wall. The maximum disturbance, $\Delta V/U_\infty = 0.12$, is quite strong compared to the base laminar boundary layer flow. On either side of this upflow are concentrated weaker flows toward the wall. The U velocity disturbance shows a decrease in U in the region of positive V, consistent with the transport of low-momentum fluid away from the wall, and an increase in U in the regions of negative V, consistent with the transport of high-momentum fluid towards the wall. The maximum U disturbance, $\Delta U/U_\infty = -0.4$, indicates that very strong disturbances are possible. The U and V velocity profiles are precisely what one would expect from a pair of streamwise counter-rotating vortices with common-flow away from the wall, having a diameter of approximately $0.55\delta^*$ (1.5 mm).

There are two significant asymmetries evident in figure 4. First, the negative V disturbance is stronger on one side. Every actuator showed, to some extent, this type of asymmetry in its flow disturbance, although the side of the disturbance which showed the stronger negative V varied among the actuators. This asymmetry was attributed to small misalignments that occurred during the fabrication procedure, which could result in the cantilever, in its non-actuated state, being slightly higher or lower than the wall, or slightly twisted with respect to the plane of the wall. The misalignment of the cantilever tip with the wall was never more than 50 μm for the actuators that were used. The misalignments, although small compared to the boundary layer length scales, were still significant compared to the cantilever amplitude and the side-gap width. This asymmetry suggests that it might be possible, with some modifications, to design an actuator that could shed a single vortex. This could be beneficial for controlling structures in a turbulent boundary layer, since the dynamically important near-wall streamwise vortices are not necessarily closely paired.

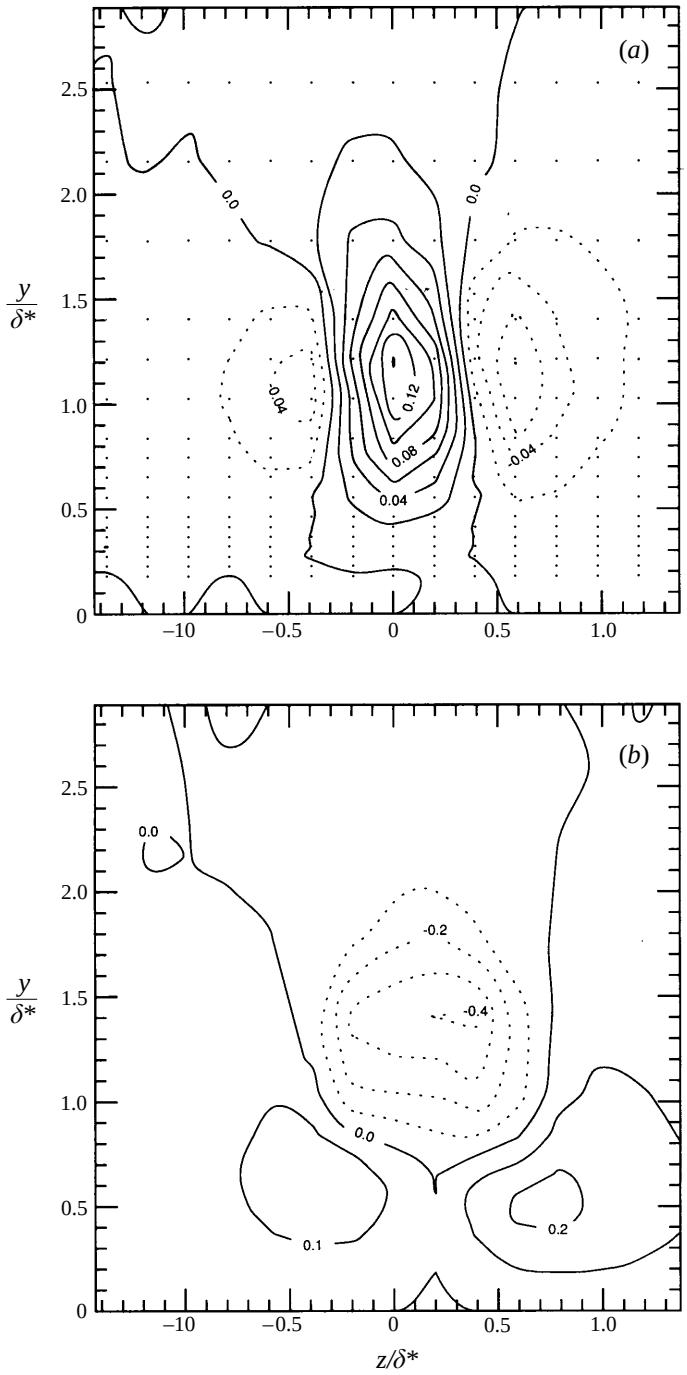

FIGURE 4. Velocity disturbance from an actuator with unequal side gaps (narrow gap at $z/\delta^* \approx 0$, wide gap at $z/\delta^* \approx 0.9$), $\Delta x/\delta^* = 4$. Flow is into the page: (*a*) $\Delta V/U_\infty$; (*b*) $\Delta U/U_\infty$.

The second asymmetry is that the spanwise location of maximum V is slightly offset from the spanwise location of minimum U. This suggests that the generated structure is slightly tilted with respect to the wall. In the flow visualization it was sometimes observed that one vortex of the pair was slightly farther from the wall than the other.

Notice also that, in the near-wall region, there is a slight positive U disturbance under the negative U disturbance. It appears that the positive U disturbances, caused by the V flow toward the wall, are encroaching underneath the negative U disturbance. This effect was generally only observed for very strong actuation amplitudes. In runs using weaker V disturbances, the negative U disturbance extended to the wall.

Figure 5 shows the velocity disturbance $4\delta^*$ downstream of an actuator with nearly equal side-gap widths (both gaps ≈ 50 μm). There is a strong positive V disturbance over both side gaps and a particularly strong negative V disturbance in the region between the side gaps. There is also a weak negative V disturbance on the outer edges of the structure. The measurements are consistent with the formation of a pair of counter-rotating vortices over each side gap, with common-flow away from the wall. However, the central two vortices complement each other to a degree where there is essentially a single strong pair of counter-rotating vortices with common-flow towards the wall, located between the side gaps. This configuration would be useful if one desired a strong controllable flow toward the wall. Comparing figure 4 with figure 5, it is clear that the gap asymmetry is a critical factor in the actuator design.

Since the unequal-gap actuator produces a simpler disturbance (a single vortex pair as opposed to two vortex pairs), it was chosen over the equal gap actuator as a better configuration for flow control. A pair of unequal-gap actuators located side by side results in a geometry similar to that of the equal-gap actuators. This configuration is used in the control results presented in § 4.

Figure 6 shows the streamwise development of the mean velocity disturbance for a typical case where the disturbance amplitude was of comparable magnitude to that used in the control runs described in the following sections. The contours were generated from a grid of data indicated by dots in figure 6(*a*). Here, the velocity signals were analog low-pass filtered at 10 Hz. Data were sampled at 200 Hz, and averaged over 1600 measurements.

In figure 6, the measurement plane is aligned in the spanwise direction with the location of the maximum positive V disturbance over the actuator (i.e. over the narrow side gap). The data in figure 6 for $\Delta x < 0$ were taken directly over the actuator narrow side gap, and hence at these points zero velocity at the test surface could not be assumed. The contouring could not be extended to the wall in this region, and the limits of the contours are indicated by a dashed line.

The growth of the V disturbance along the length of the cantilever is evident in figure 6(*a*). The cantilever extends from its fixed end boundary condition at $\Delta x/\delta^* = -7.5$ to its tip at $\Delta x/\delta^* = 0$. The V disturbance was first measurable at $\Delta x/\delta^* \approx -3.2$, reaching 70% of its maximum value at $\Delta x/\delta^* \approx -1.3$. The V disturbance maximum appeared to occur close to the tip of the actuator. The V disturbance is substantial for at least $6\delta^*$ in the streamwise direction, and is at a maximum at about $0.4\Delta^*$ in the wall-normal direction, indicating an aspect ratio (L/D) for this disturbance of order 10. In general, for the generated disturbance, the length will scale like the length of the actuator, and the diameter will scale with the forcing level.

The velocity measurements are consistent with the flow visualization observations

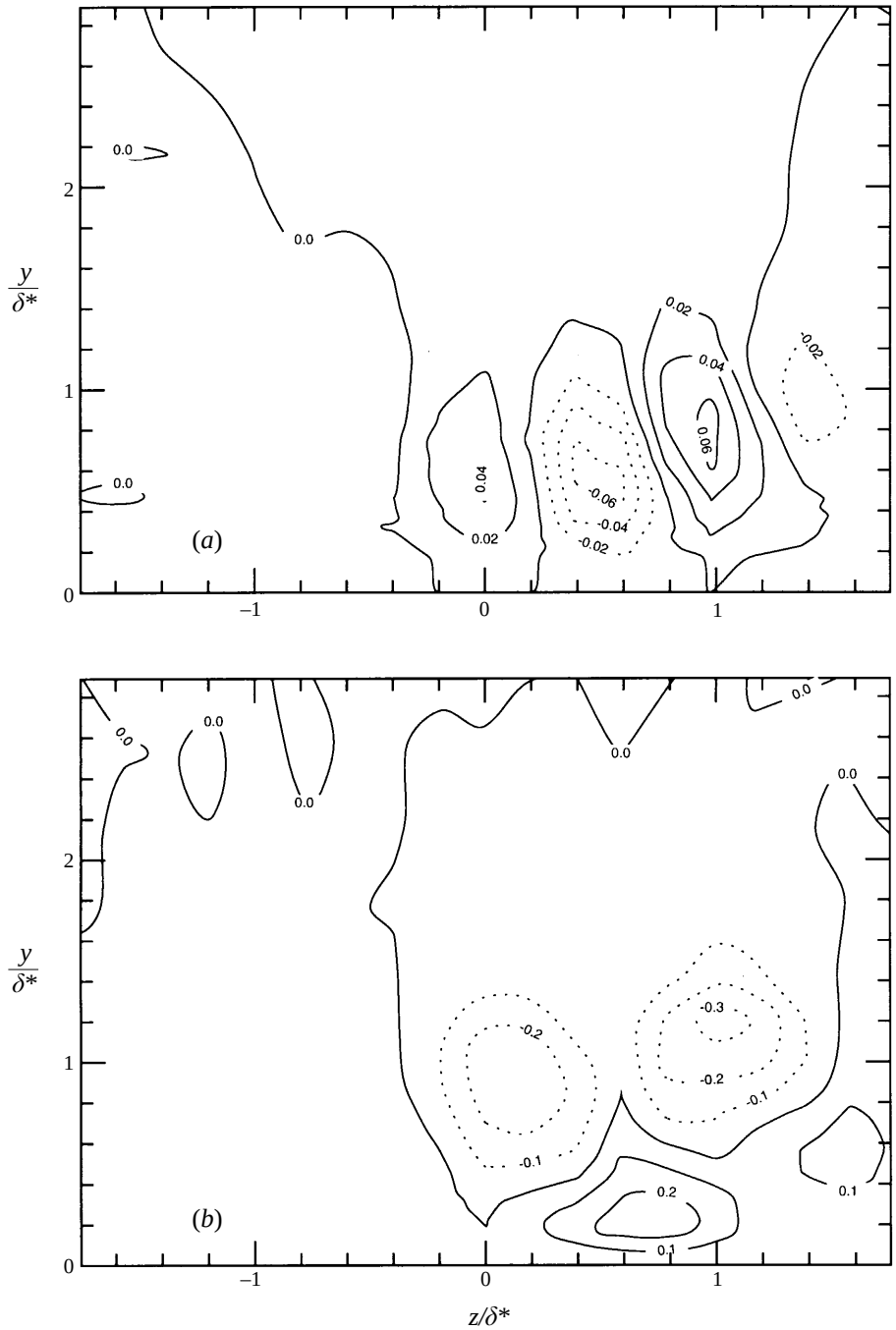

FIGURE 5. Velocity disturbance from an actuator with equal side gaps (gaps at $z/\delta^* \approx 0, 0.9$). $\Delta x/\delta^* = 4$: (*a*) $\Delta V/U_\infty$; (*b*) $\Delta U/U_\infty$.

presented earlier, where the structure was observed only over the last 5 mm ($1.9\delta^*$) of the cantilever. The strong V disturbance over the actuator is responsible for the dye plume observed in figure 3. These results are also consistent with the concept discussed earlier that there is an additive effect as the actuator disturbance convects

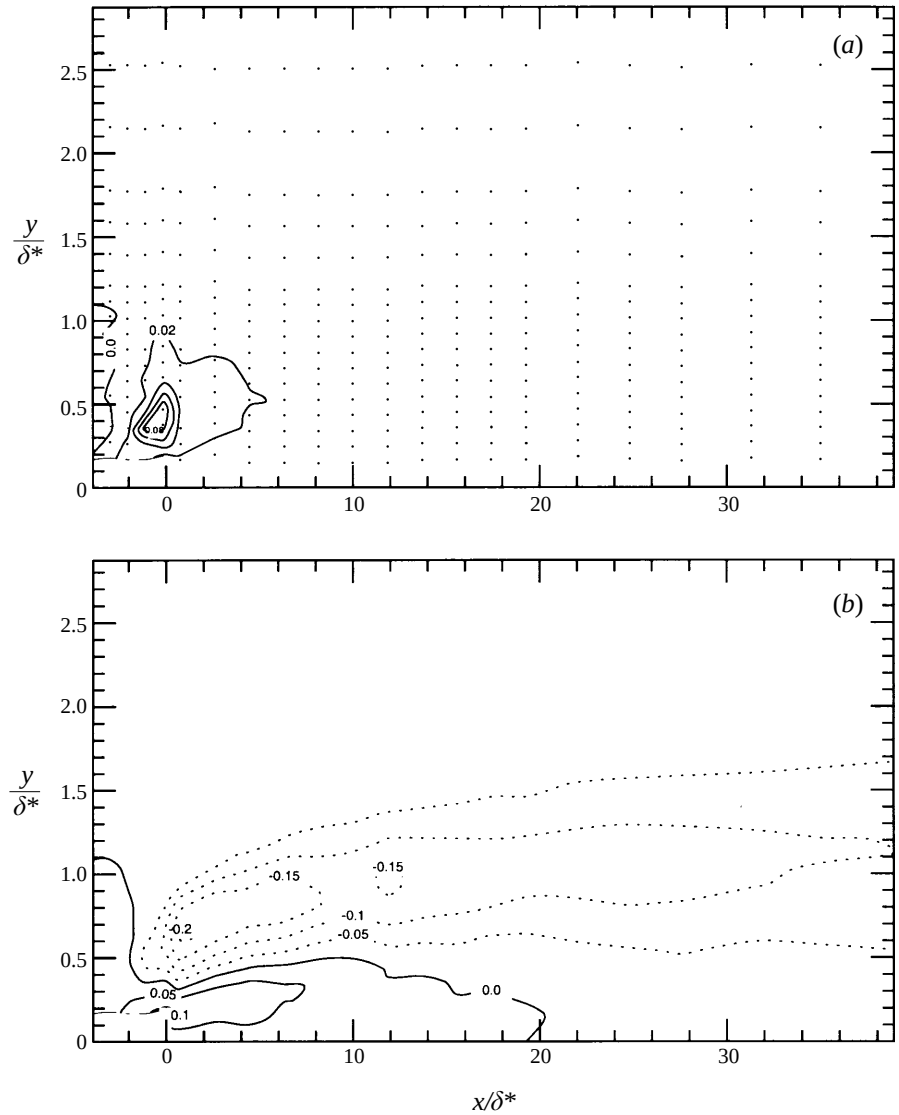

FIGURE 6. Actuator velocity disturbance. Measurement plane aligned with the actuator narrow gap: (*a*) $\Delta V/U_\infty$; (*b*) $\Delta U/U_\infty$.

downstream along the side gap, and is acted on multiple times as the cantilever oscillates.

The V disturbance weakens rapidly downstream of the actuator tip, and is essentially gone by $\Delta x/\delta^* = 10$. This decay is too rapid to be accounted for by stretching or viscous diffusion in a laminar boundary layer. We suspect that this effect results from mixing produced by unsteadiness in the flow caused by the oscillating actuator. As will be shown in the next section, u and v velocity fluctuations exist over the actuator and persist downstream. The most rapid decay of the vortex structure occurs in the regions of the largest fluctuations. Although we did not measure w, one suspects that there are comparable w velocity fluctuations as well. As the measured r.m.s. velocity fluctuations are smaller than the mean disturbance, we claim the pro-

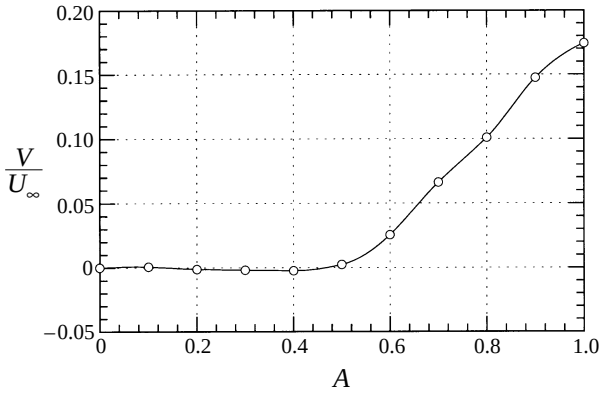

FIGURE 7. Actuator-induced wall-normal velocity as a function of the actuator drive amplitude. $\Delta x/\delta^* = 0.0$, $y/\delta^* \approx 0.50$, centred over the actuator narrow gap.

duction of a 'quasi-steady' pair of vortices. Nevertheless, the flow clearly is unsteady and the velocity fluctuations provide a means for small-scale momentum transport. As the actuator generated a nearly symmetric pair of counter-rotating vortices, the net circulation added to the flow is close to zero; mixing could rapidly weaken this structure, particularly just downstream of the actuator where the structure production mechanism is gone. A more full understanding of this phenomenon requires further investigation.

The U disturbance produced by the vortex pair was considerably stronger than the V disturbance, and persisted much farther downstream. A small positive U disturbance also appeared in the near-wall region close to the actuator tip, due to the slight misalignment that occurred between the maximum positive V (which this data set is aligned with) and the maximum negative U (see, for instance, figure 4). Measurements taken at a small spanwise offset from the plane of this data set showed a negative U disturbance extending to the wall, even close to the actuator tip.

Figure 7 shows measurements of V as a function of the actuator drive amplitude, where A is the drive amplitude in volts, non-dimensionalized by its maximum value of 25 V. Measurements were taken at the actuator tip, aligned with the narrow side gap. The distance from the wall of maximum V did not vary much with increasing amplitude. Measurements are shown at the same y location. Note that there is no measurable velocity disturbance below an actuator amplitude $A = 0.5$. This likely results from viscous effects. For $A > 0.5$, V increases nearly linearly.

2.3.3. *Velocity fluctuations*

Operation of the actuator produces velocity fluctuations at the drive frequency, at harmonics and at zero frequency by nonlinear interaction, and over a broad band of relatively low frequencies, presumably arising from nonlinear interactions with other disturbances in the flow. Power spectra measurements performed close to the actuator tip (within $\Delta x/\delta^* \approx 0.7$, $\Delta z/\delta^* \approx \pm 0.35$) showed peaks at the drive frequency; however in all cases, the peaks were small. The drive frequency peak was largest for the measurements closest to the wall ($y/\delta^* = 0.23$). For these near-wall measurements, an integration of the fluctuating energy in the peak at the drive frequency gave a value of $(\langle uu \rangle + \langle vv \rangle)/U_\infty^2 = O(10^{-6})$. This shows that there is very little energy in the flow at the drive frequency, even very close to the actuator. Recall that the drive frequency approximately corresponds to the actuator resonance frequency. The actuator was

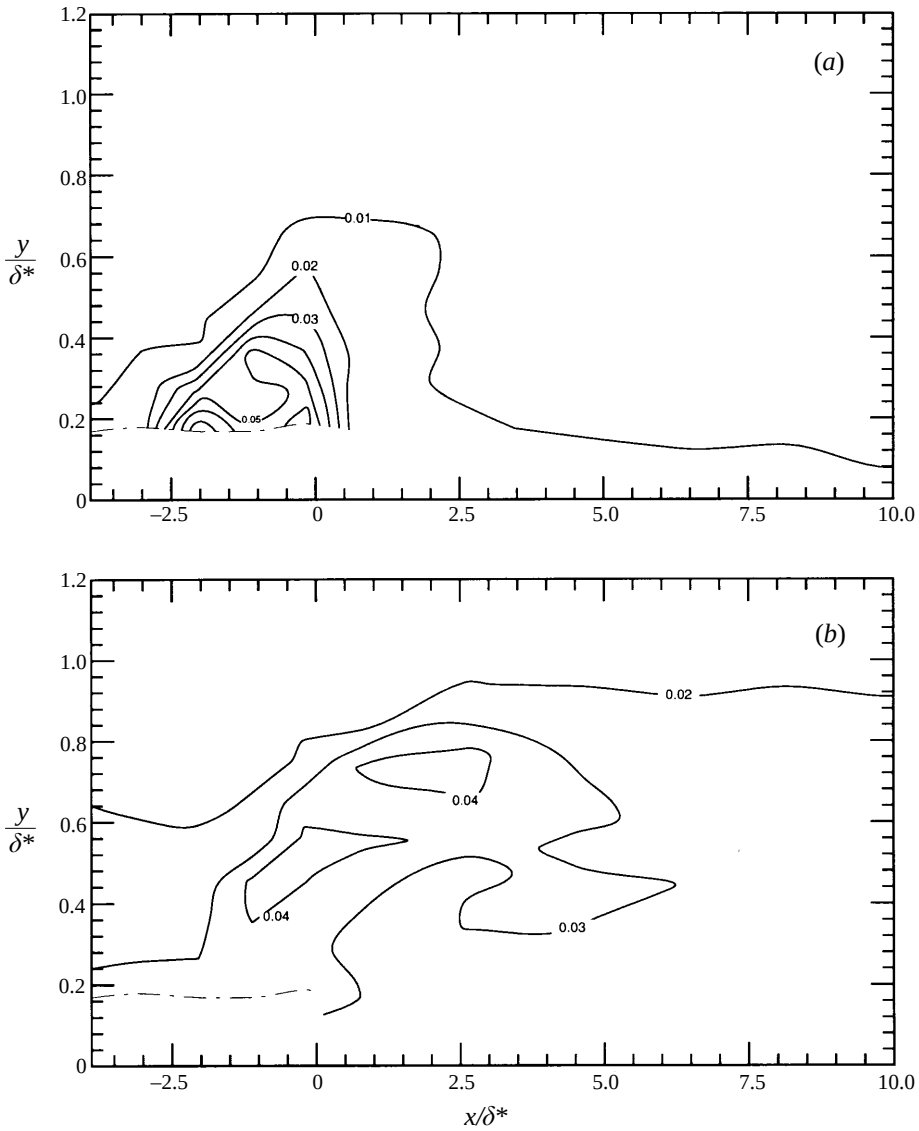

FIGURE 8. Actuator disturbance r.m.s. velocities. Measurement plane aligned with the actuator narrow gap: (*a*) v_{rms}/U_∞; (*b*) u_{rms}/U_∞.

designed so that its resonance frequency was high compared to frequencies which typically persist in the low-speed water boundary layer that was used.

Figure 8 shows r.m.s. velocity contours aligned with the actuator narrow side gap. The mean velocity data for this run were shown earlier in figure 6. The results are shown only in the neighbourhood of the actuator, which is the only region where the r.m.s. velocities were sizeable. Instrument noise generated apparent r.m.s. fluctuations of about $0.01U_\infty$ on v and $0.02U_\infty$ on u. The only significant v_{rms} is directly over the actuator tip, where it is expected. However, the fluctuations weaken away from the wall and almost immediately downstream of the actuator. The u_{rms} is only about 10–20% of the mean U disturbance of figure 6 and is never much larger than the

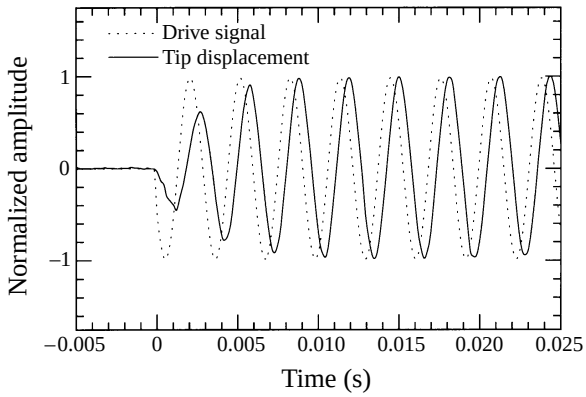

FIGURE 9. Actuator step response, driven.

instrument noise in the u signal. Comparing figure 6 with figure 8, it is clear that the main disturbance from the actuator is a quasi-steady phenomenon.

2.3.4. *Step response and tip displacement*

In understanding the dynamics of the actuator disturbance, it is important to look at both the response of the actuator cantilever and the response of the flow. Figure 9 shows the drive-amplitude step response of the actuator cantilever tip in the wall-normal direction. The tip displacement signal is a time trace from a photodiode measuring the position of a HeNe laser beam reflected off the actuator tip. Figure 9 also shows a time trace of the actuator drive signal. Both signals are normalized by their maximum amplitude. The rise time of the cantilever tip is approximately 6 ms, which is two cycles of the drive signal.

The tip displacement measurement system found a maximum tip displacement amplitude (zero-to-peak) of 130 ± 15 μm, when the actuator was driven at its resonance frequency with a signal of amplitude 25 V ($A = 1$). Thus, for typical operating conditions, the tip displacement amplitude was $\leqslant 5\%$ of the boundary layer displacement thickness of the external flow. Surface roughness of dimension equal to the tip displacement amplitude would be considered aerodynamically smooth at the Reynolds number of this flow.

Measurements of the flow step response (see JR) at the actuator tip showed a measurable disturbance developing within 120 ms, with the disturbance reaching a steady state within 250 ms, corresponding to approximately $3t_{f\infty}$. This seems reasonable when one considers that the actuator disturbs the flow along some length of the side gap, and the generated disturbance will convect at some fraction of the free-stream velocity. Thus, the actuator should be able to respond quickly enough to interact with any structure in the flow, so long as the lifetime of the structure is longer than the time it takes that structure to convect over the actuator.

2.4. *Power consumption*

The current through the actuator was generally about 70° out of phase with the driving voltage. This phase difference is a sign of the strong capacitive nature of this type of actuator. In fact, the health of an actuator could generally be tracked by monitoring its capacitance.

The deviation in the phase difference from the 90° phase difference of an ideal capacitor is indicative of the actuator's power consumption. Using the phase difference

between the driving current and voltage, along with their r.m.s. values, the actuator power consumption was found to be $P \approx 0.6$ mW for a typical actuator at maximum amplitude.

A non-dimensional power factor, π, can be defined as the ratio of the actuator power to the local skin friction drag power integrated over the associated control area:

$$\pi = \frac{P}{\rho A_c^+ U_\infty v^2}, \tag{2.1}$$

where A_c^+, defined in § 1 as the control area associated with an actuator, is on the order of 4000, and ρ is the fluid density. Substituting into equation (2.1) results in a power factor $\pi \approx 500$.

The power factor is clearly several orders of magnitude larger than that necessary for using this actuator in a control system aimed at producing a net skin friction drag reduction. However, before dismissing this actuator as a candidate for drag reduction control, several factors can be listed in its favour. First, the current actuator was not optimized for low power consumption; different materials or fabrication techniques might help bring down the power consumption. Second, the actuator will not operate steadily, nor will it always operate at max power; thus this power factor should be viewed more as an upper bound. Third, the actuator was tested in a relatively low-drag flow; equation (2.1) shows that increasing U_∞ will reduce the power factor. Fourth, the choice of A_c^+ was somewhat arbitrary; if the control effects persist farther downstream than the streamwise extent of the control module, A_c^+ will increase, reducing the power factor. Finally, power dissipation in the actuator, as opposed to work done on the fluid, should scale with the volume of the cantilever, while skin friction drag is associated with a surface area; operation at larger Reynolds numbers would require a reduction in the size of the actuator, reducing the actuator power consumption faster than the associated skin friction. Hence, we feel it is too early to rule out this particular actuator design for use in net skin friction drag reduction control.

3. Transition delay

3.1. *Overview*

This section describes an experiment concerned with delaying the transition produced by a cylinder protruding from the wall in a laminar boundary layer. The cylinder acts as a localized, finite-amplitude, three-dimensional disturbance. It generates a relatively strong-amplitude velocity perturbation, particularly in the streamwise component. The region of flow affected by the cylinder spreads laterally downstream, and is commonly referred to as a turbulent wedge.

The main disturbance from the cylinder which the actuator aimed to control were a pair of streamwise vortices, along with the high- and low-speed streaks that the vortices produced. The vortices form when the boundary layer spanwise vortex tubes are wrapped around the protruding cylinder and stretched by the downstream convection on either side. The vortex pair has common flow towards the wall. Figure 10 shows a sketch of this process. The vortices transport x-momentum resulting in alternating low- and high-speed streaks near the wall. Figure 11 shows a measurement of the mean velocity disturbance downstream of the cylinder, which is consistent with the formation of a pair of streamwise vortices.

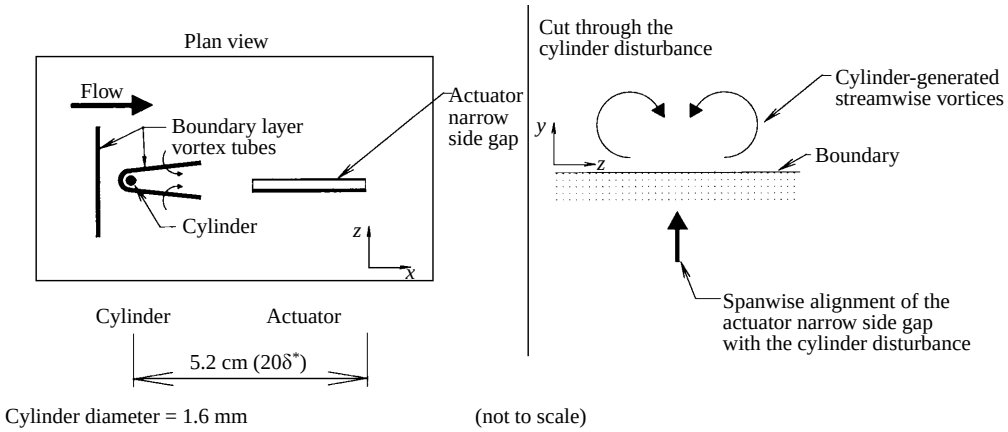

FIGURE 10. Transition control experimental setup.

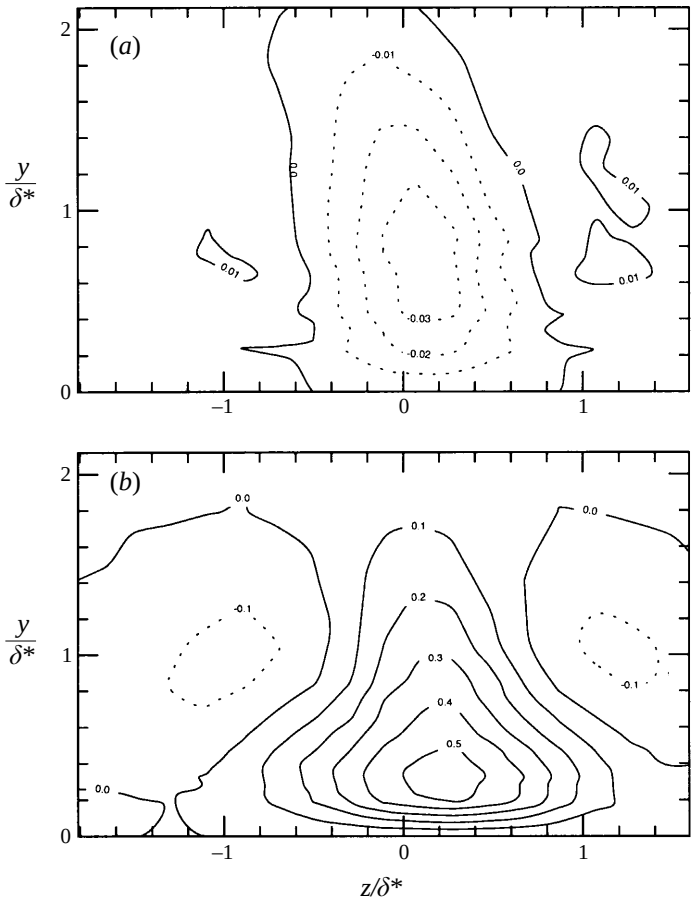

FIGURE 11. Cylinder flow disturbance, (z, y)-plane, $20.4\delta^*$ downstream of the cylinder. Cylinder is located at $z/\delta^* \approx 0$: (*a*) $\Delta V/U_\infty$; (*b*) $\Delta U/U_\infty$.

3.2. *Background*

The goal of transition control is to attenuate flow disturbances so as to maintain near-laminar flow. This requires proper phasing and amplitude of the counter-disturbance. A number of previous experiments have been performed with this in mind. Transition control was a logical first step for near-wall active boundary layer control due to the relationship between transition and Tollmien–Schlichting (TS) waves. The two-dimensional nature of TS waves allows cancellation using a simple linear wave superposition technique. The counter-disturbance wave has been generated using wall motion (Schilz 1965/66; Gedney 1983), a vibrating wire (Milling 1981; Thomas 1983) and surface heaters (Liepmann, Brown & Nosenchuck 1982). In all of these examples, the phase of the cancelling wave generator was tuned to achieve maximum attenuation of the TS wave. However, complete cancellation was not achieved. Thomas suggested that weak background three-dimensional disturbances, which interacted with the primary two-dimensional disturbance, prevented complete cancellation.

There are alternative routes to turbulence besides the evolution of two-dimensional TS waves. Laminar boundary layers are also susceptible to inviscid instabilities such as those caused by inflection points in a velocity profile. Inflections in both the wall-normal and spanwise profiles of streamwise velocity can lead to instabilities that can grow significantly faster than a TS wave. Furthermore, localized three-dimensional disturbances can also lead directly to turbulence. Breuer & Haritonidis (1990) and Breuer & Landahl (1990) investigated the evolution of localized three-dimensional disturbances, showing that they can have considerably larger growth rates than two-dimensional wave disturbances. This work was extended in Breuer & Kuraishi (1993), who point out that in real engineering situations, a laminar flow is likely to be subjected to three-dimensional disturbances from sources including surface irregularities. Breuer, Haritonidis & Landahl (1989) investigated the control of a large-amplitude three-dimensional disturbance in a laminar boundary layer. The initial disturbance was generated by a controllable wall bump that flexed out into the flow. The disturbance was counteracted downstream by a streamwise array of eight smaller controllable wall bumps. They showed that with proper phasing, they could delay the initial disturbance breakdown to a turbulent spot by about 50 displacement thicknesses.

In a related experiment, Blackwelder & Liu (1994) used a controllable delta-wing vortex generator to introduce streamwise vortices into the boundary layer that were counter to Görtler streamwise vortices introduced with a curved flow section upstream. With proper alignment, they were able to delay the breakdown of the Görtler vortices.

The experiment described in this section complements the previous work of Breuer *et al.* (1989) and Blackwelder & Liu (1994). The delay of transition from a three-dimensional finite-amplitude disturbance is shown. However, a different disturbance and a different type of actuator is used for the control reported here.

3.3. *Setup*

The experimental setup is shown in figure 10. A cylinder was installed upstream of, and aligned with, the actuator narrow side gap. The cylinder extended through the boundary layer. The actuator tip was 51 cm downstream of the boundary layer leading edge. The free-stream velocity of the boundary layer was 0.20 m s^{-1}. The start of transition with respect to the leading edge, x_t, depended on U_∞, $x_\circ$, d, and ν, where $x_\circ = 45$ cm is the cylinder location from the leading edge and $d = 1.6$ mm is the cylinder diameter. Transition was also affected by the noise in the free stream (free-stream turbulence intensity < 0.006). For the results presented here, the transition

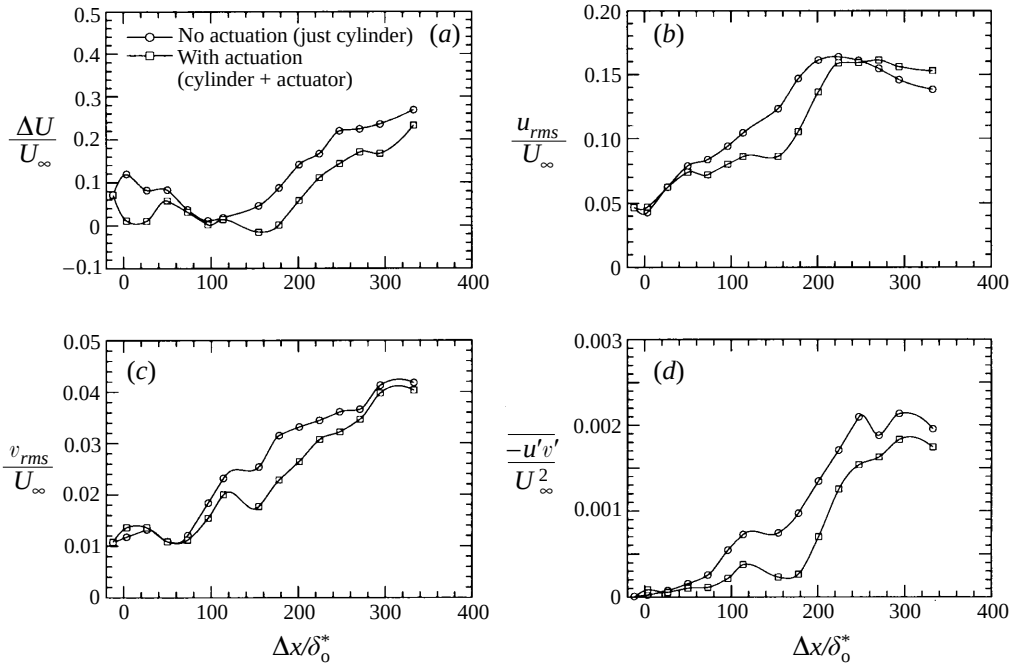

FIGURE 12. Transition delay, streamwise profile, $y/\delta^* \approx 0.5$, $z/\delta^*_\circ = 0$: (*a*) ΔU; (*b*) u_{rms}; (*c*) v_{rms}; (*d*) $-\overline{u'v'}$.

began at $Re_t = U_\infty x_t/\nu \approx 130\,000$, approximately $100\delta^*_\circ$ downstream of the cylinder, where $\delta^*_\circ = 2.6$ mm was the measured displacement thickness of the undisturbed flow at the location of the cylinder.

A steady actuator drive amplitude of $A = 1.0$, the maximum allowable amplitude for this actuator design, was found to maximize the reductions in the measured statistics in the transitional region. All results presented in this section were performed with $A = 1.0$. A short-time test was also performed at $A = 1.2$, which gave slightly better results than at $A = 1.0$, suggesting that a greater transition delay than that shown below might have been possible.

The spanwise location of the actuator narrow side gap was initially aligned with the cylinder. The cylinder spanwise location was then adjusted slightly to maximize the reductions in the measured statistics resulting from the control in the transitional region. The effect of the cylinder/actuator alignment on the control is addressed later in this section. Note, though, that a comparison of figures 4 and 11 shows that the spanwise extent of the cylinder vortices is larger than that of the actuator vortices. The small difference in free-stream velocity for these two plots has little effect on the spanwise scales of the disturbances. This indicates that the interaction between the cylinder vortices and the control vortices is not a simple cancellation, and alignment issues should be important.

3.4. *Results*

Figure 12 shows the effect of steady actuator control on the cylinder disturbance as the disturbance developed in the streamwise direction. The streamwise position is given with respect to the actuator tip, with the cylinder located at $\Delta x/\delta^*_\circ = -20$. These measurements were taken aligned with the actuator narrow side gap, at a local

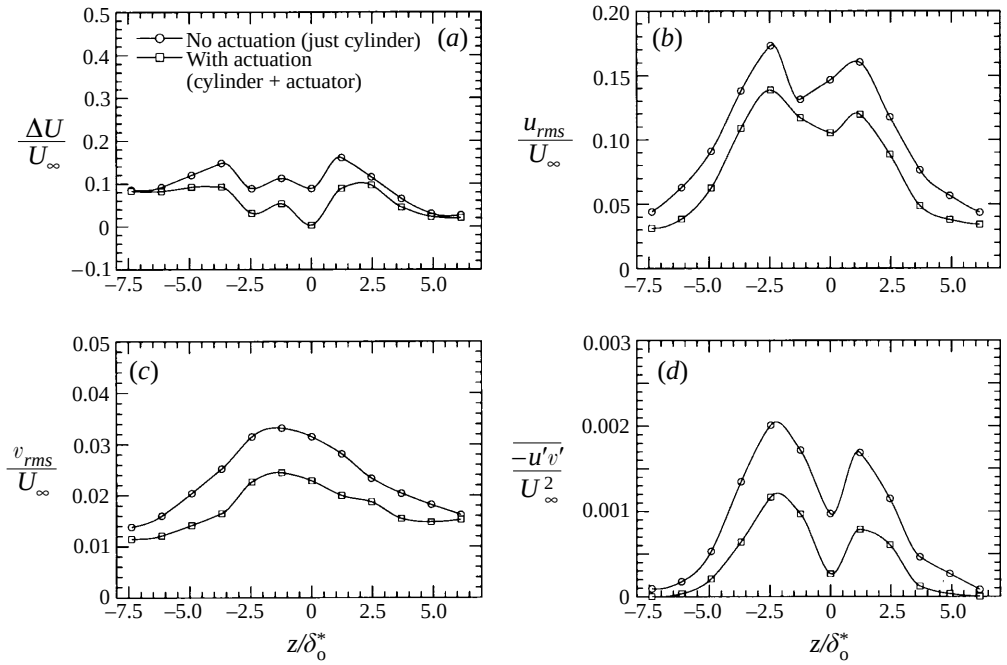

FIGURE 13. Transition delay, spanwise profile, $\Delta x/\delta_\circ^* = 178$, $y/\delta^* \approx 0.5$: (*a*) ΔU; (*b*) u_{rms}; (*c*) v_{rms}; (*d*) $-\overline{u'v'}$.

distance from the wall corresponding to $U/U_\infty = 0.3$. This local distance from the wall, equivalent to $y/\delta^* \approx 0.5$, was the same value used by Breuer *et al.* (1989) in presenting their results. The velocity signals were analog low-pass filtered at 20 Hz, and sampled at 50 Hz.

Large data sets were necessary to get the fluctuation statistics to converge. The statistics measured included the U disturbance, u_{rms}, v_{rms} and $-\overline{u'v'}$. Data were taken in groups of 3000 points, and the statistics were considered converged when an additional set of 3000 data points changed the statistics by less than 1%. Generally, the Reynolds stress term was the slowest to converge. In the relatively steady region close to the cylinder, 21 000 samples were needed. In the unsteady region, as many as 42 000 samples were needed. In order to be sure that the differences measured between the cases with and without control were actual differences and not a result of slow variations in the tunnel flow parameters, collection of each 3000 data point group was alternated between the two cases at each location.

In figure 12(*a*), the initial increase in the U disturbance downstream of the cylinder is evident for the no control case (data were taken in the region of the disturbance with common-flow towards the wall). The initial U disturbance decays until about $\Delta x/\delta_\circ^* \approx 80$, at which point it starts to grow as the disturbance begins to break down. By $\Delta x/\delta_\circ^* = 80$, the uncontrolled cylinder disturbance is of the same amplitude as the controlled case. However, further downstream it is clear that the control has had a significant effect. For each of the statistics shown in figure 12, the breakdown of the cylinder disturbance is pushed downstream by approximately $40\delta_\circ^*$ for the case with actuation, as compared to the case with no actuation. This is comparable to the results obtained by Breuer *et al.* (1989) and Blackwelder & Liu (1994).

To obtain a better understanding of the range of the control effect on the dis-

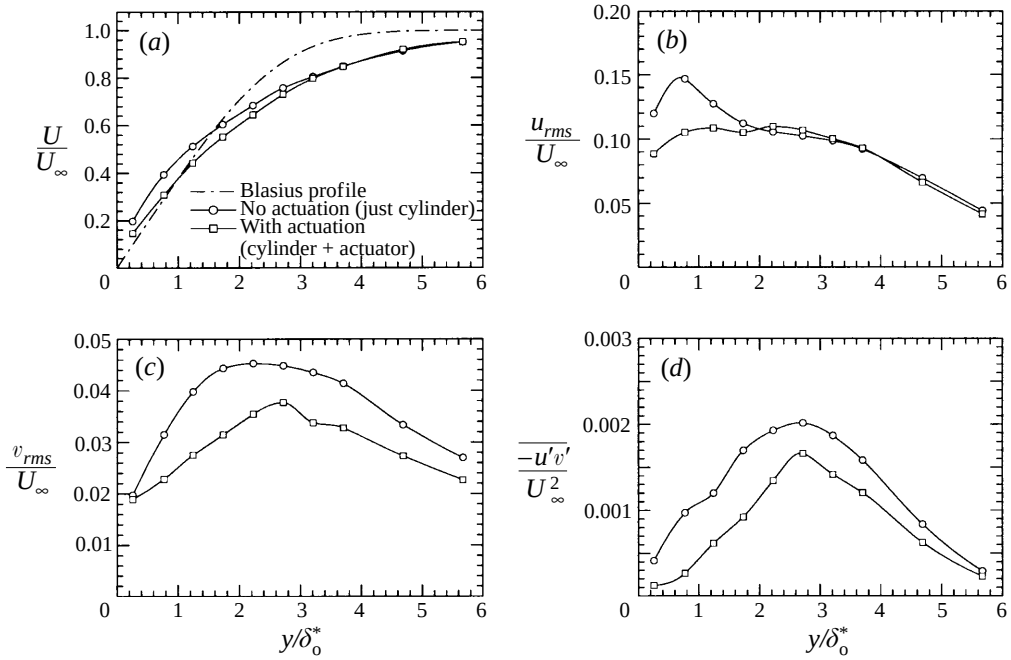

FIGURE 14. Transition delay, wall-normal profile, $\Delta x/\delta_\circ^* = 178$, $z/\delta_\circ^* = 0$: (*a*) U; (*b*) u_{rms}; (*c*) v_{rms}; (*d*) $-\overline{u'v'}$.

turbance breakdown, spanwise and normal traverses were performed. As with the previous run, at each data location, samples were taken until the statistics converged. Figure 13 shows results from a spanwise traverse taken in the transitioning region at $\Delta x/\delta_\circ^* = 178$ and $y/\delta^* \approx 0.5$. The actuator narrow side gap was aligned with $z/\delta_\circ^* = 0$. Data were taken across the span of the wedge generated by the cylinder. The data show a consistent reduction in the disturbance amplitude, velocity fluctuations, and Reynolds stress in the central region of the disturbance. Figure 14 shows results from a wall-normal traverse in the transitioning region at $\Delta x/\delta_\circ^* = 178$ and $z/\delta_\circ^* = 0$. The reduction in each of the statistics extends nearly through the boundary layer. The data indicate that the actuator control had a profound effect on the development of the cylinder disturbance, extending throughout the region of flow affected by the disturbance.

It was of interest to see how much misalignment of the actuator, with respect to the cylinder, could be tolerated before the transition delay effect disappeared. The cylinder mount could be moved off centre in the spanwise direction. Data were taken with the cylinder moved in the negative spanwise direction only (the results for the other direction should be symmetric). Figure 15 shows control results at $\Delta x/\delta_\circ^* = 178$, $y/\delta^* \approx 0.5$, and $z/\delta_\circ^* = 0$, as a function of the cylinder position c normalized by the cylinder diameter. At $\Delta c/d = 0$, the cylinder was aligned with the actuator narrow side gap. The LDA measuring volume was maintained at $z/\delta_\circ^* = 0$ so that it was always aligned with the actuator narrow side gap. As the cylinder was moved off alignment with the actuator, not only was a reduction in the statistics maintained, but the largest reduction occurred at $\Delta c/d \approx -1$. In fact, the measurements shown in figures 12–14 were done with $\Delta c/d \approx -1$. As was explained earlier, the cylinder was lined up with the actuator and then adjusted slightly to maximize the control

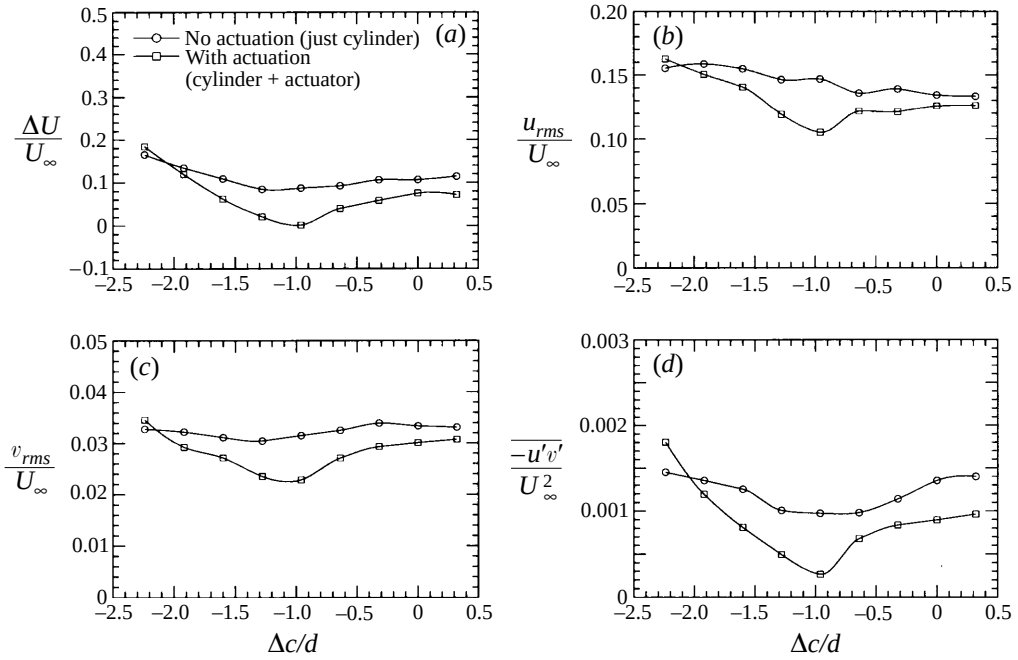

FIGURE 15. Transition delay, cylinder/actuator misalignment, $\Delta x/\delta^*_\circ = 178$, $y/\delta^* \approx 0.5$, $z/\delta^*_\circ = 0$: (*a*) ΔU; (*b*) u_{rms}; (*c*) v_{rms}; (*d*) $-\overline{u'v'}$.

effect. Figure 15 shows that for misalignments out to $\Delta c/d \approx -2$ the actuator control continued to produce a delay in the development of the statistics.

Figure 16 shows the results of a spanwise traverse measuring U and V just downstream of the actuator tip ($\Delta x/\delta^*_\circ = 3$). For this run, the cylinder was aligned with the actuator such that $\Delta c/d = -1$, the alignment that gave the best results in figure 15. Figure 16 indicates that this position has the actuator disturbance aligned approximately with an inflection point in the U and V profiles resulting from the cylinder disturbance. Since the actuator disturbance was smaller in spanwise scale than the cylinder disturbance, the alignment to counteract an inflection point required the actuator disturbance to be aligned off centre of the cylinder disturbance.

4. Control of steady and unsteady streaks

4.1. *Overview*

This section describes experiments investigating the control of steady and unsteady disturbances generated with an array of spanwise suction holes using a single spanwise array of actuators. The suction holes have a similar effect on the flow as the cylinder of the previous section. Localized sections of spanwise vortex tubes in the boundary layer are trapped by the suction holes; the remainder of the vortex tube is stretched by downstream convection. When multiple suction holes are used, arrays of horseshoe vortices are produced.

The generation of horseshoe vortices by suction holes is a well known phenomenon. Figures 99 and 100 of Van Dyke (1982) show smoke visualization photographs of this vortex generation technique taken by Bradshaw. Gad-el-Hak & Hussain (1986) used pulsed suction to generate horseshoe vortices, which they found would lift and

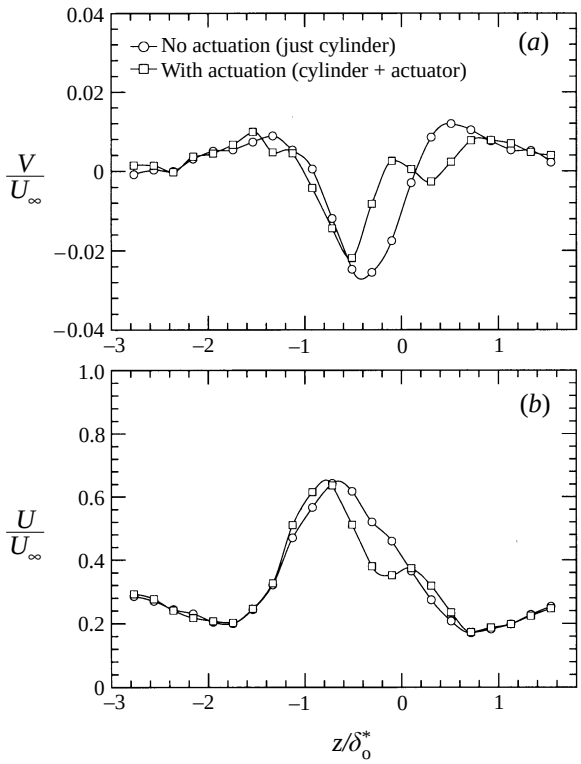

FIGURE 16. Spanwise profile of cylinder disturbance, with and without actuation. $\Delta x/\delta^*_\circ = 3$, $y/\delta^* \approx 0.5$, $\Delta c/d = -1$. (*a*) V/U_∞; (*b*) U/U_∞.

ultimately break down. Gad-el-Hak & Blackwelder (1987) then successfully eliminated the pulsed suction disturbance using a suction actuator. Part of their success can be attributed to the location of their suction actuator immediately downstream of the pulsed suction disturbance generator, allowing the actuator to cancel the disturbance before it had much chance to affect the streamwise velocity. For the experiments described in this section, the suction-hole disturbance was allowed to mature prior to reaching the actuator, making it more difficult to attenuate.

Gad-el-Hak & Hussain (1987) also found that suction through a spanwise hole array at low suction rates produced arrays of steady vortices, while at high suction rates there was a periodic shedding of the vortices. For the experiments described here, all unsteadiness in the suction disturbance was generated by pulsing the suction; the suction rate was set so that steady suction developed steady streamwise vortices.

The suction holes offered two main advantages over the cylinder used in the previous section. First, the suction holes could be connected to solenoid valves, allowing simple generation of unsteady disturbances. Second, the disturbance size was controllable by adjusting the suction rate and the separation between the suction holes. The suction disturbance could then be tailored to be closer in scale to the actuator counter-disturbance than was possible for the cylinder disturbance.

4.2. *Setup*

Four 0.4 mm diameter suction holes were used to generate the flow disturbance. The combined flow through all four suction holes was set to approximately 1.6 ml s^{-1}.

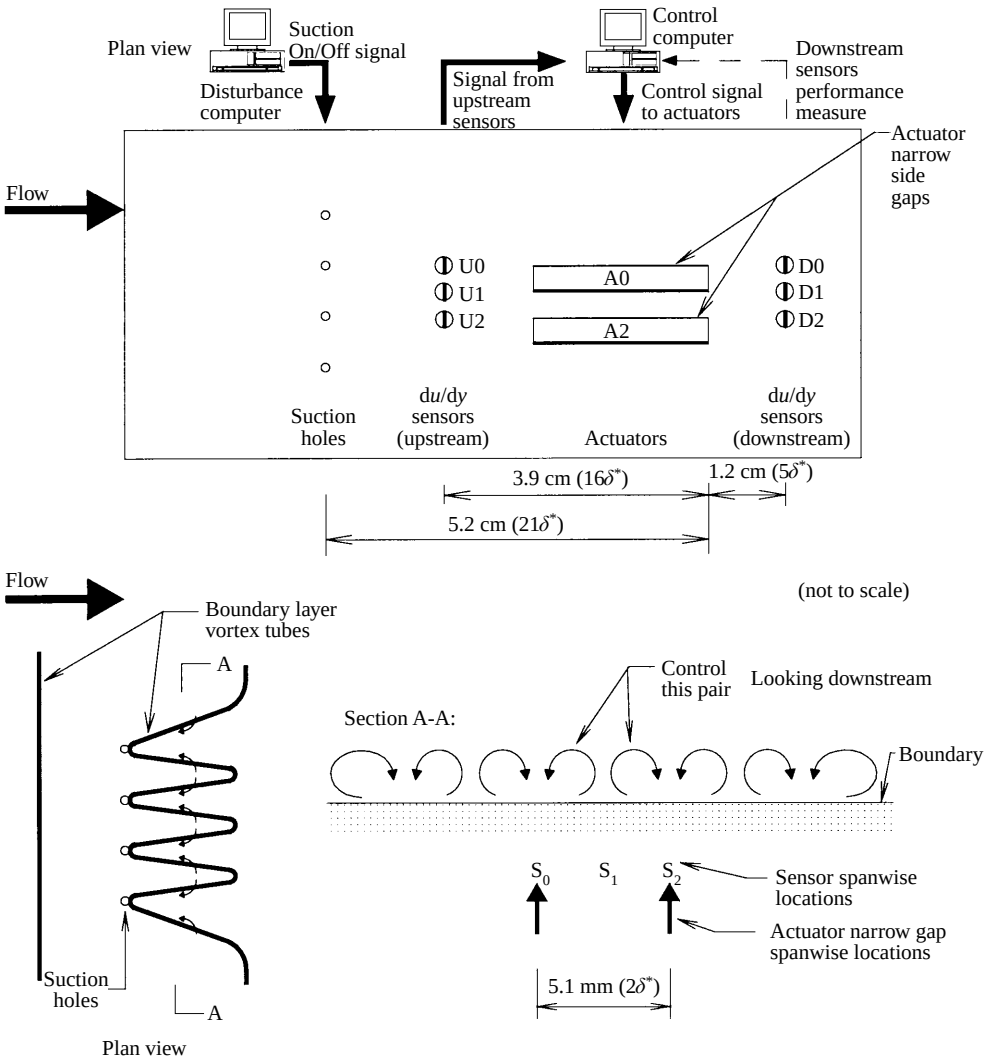

FIGURE 17. Suction hole disturbance experimental setup.

The pressure head of the tunnel ($\approx$ 30 kPa) allowed this flow rate to be achieved by exhausting, through an adjustable orifice, to atmospheric pressure. The bleed flow exhausted into a water-filled container in which a constant head was maintained.

The periodic vortex shedding from suction holes is a function of the free-stream velocity. Increasing the free-stream velocity resulted in the transition from periodic to steady vortex generation occurring at higher suction rates. The results presented in this section were performed with a free-stream velocity of U_∞=0.26 m s^{-1}, which provided a strong, steady flow disturbance from the suction holes. At this condition, the displacement thickness at the actuator tip was measured to be 2.5 mm. This value is used for normalizing length scales in this section.

The four suction holes generated eight streamwise vortices, although the focus of the control experiment described here was the central vortex pair. The extra vortices were generated to ensure that the central vortices had comparable dimensions. The central vortex pair had common-flow away from the wall. Since a single actuator

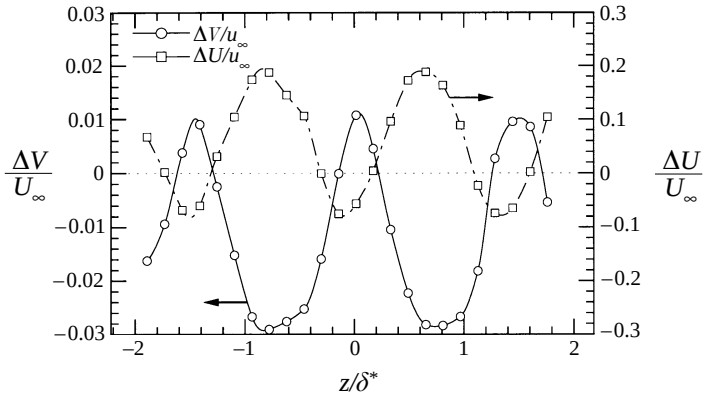

FIGURE 18. Spanwise velocity profile of the suction disturbance $2\delta^*$ downstream of the suction holes, $y/\delta^* = 0.4$: $\Delta V/U_\infty$ and $\Delta U/U_\infty$.

produced a vortex pair with common-flow away from the wall as well, control of the suction flow disturbance required the coordinated use of two spanwise-adjacent actuators to form, between them, a vortex pair with common-flow towards the wall. Figure 17 illustrates this configuration along with other aspects of the experimental setup.

The actuator tip was 51 cm downstream of the boundary layer leading edge. Spanwise arrays of hot-film wall shear sensors (oriented to measure the streamwise component of wall shear) were located upstream and downstream of the actuators. The sensors and actuators are labelled in figure 17 to assist in identification. The sensor arrays were aligned so that during a suction disturbance, the sensors labelled 0 and 2 would measure a relative shear increase, and the sensors labelled 1 would measure a relative shear decrease.

Figure 18 shows a spanwise profile of the U and V velocity disturbances taken $2\delta^*$ downstream of the suction holes at $y/\delta^* = 0.4$. Means were formed from 2048 data points sampled at 200 Hz. The suction holes were located at $z/\delta^* \approx \pm 1.0, \pm 3.0$. Figure 18 shows flow toward the wall nearly aligned with the suction holes, and flow away from the wall centred between the suction holes, as expected. Momentum transport by the V disturbance produced low- and high-speed streamwise-momentum streaks. The V disturbance was weak, and decayed rapidly. The primary disturbance over the actuators and sensors was the streamwise streaks. The r.m.s. velocities were small and within the range of measurement system electronic noise, indicating that the suction disturbance was essentially steady so long as suction was steady.

Figure 19(a) shows sensor measurements phase-averaged over 32 pulsed suction disturbance cycles, with no actuation. The wall shear data are normalized by the undisturbed flow wall shear ($\tau_\circ$). The period of each cycle, t_d, was 4 s, with the suction disturbance period equal to half of the full cycle. The timing of this disturbance is on the order of typical disturbance lifetimes for a flow of this Reynolds number. Data were sampled at 50 Hz, resulting in 200 data samples per cycle. Shortly after the suction disturbance was initiated, sensors U0 and U2 show the expected large increase in shear. However, sensor U1 shows a slight increase in shear rather than the decrease that would be expected. This results from the removal of some of the boundary layer by the suction, increasing the streamwise shear compared to the undisturbed boundary layer. Later in the cycle, the downstream sensors detect the

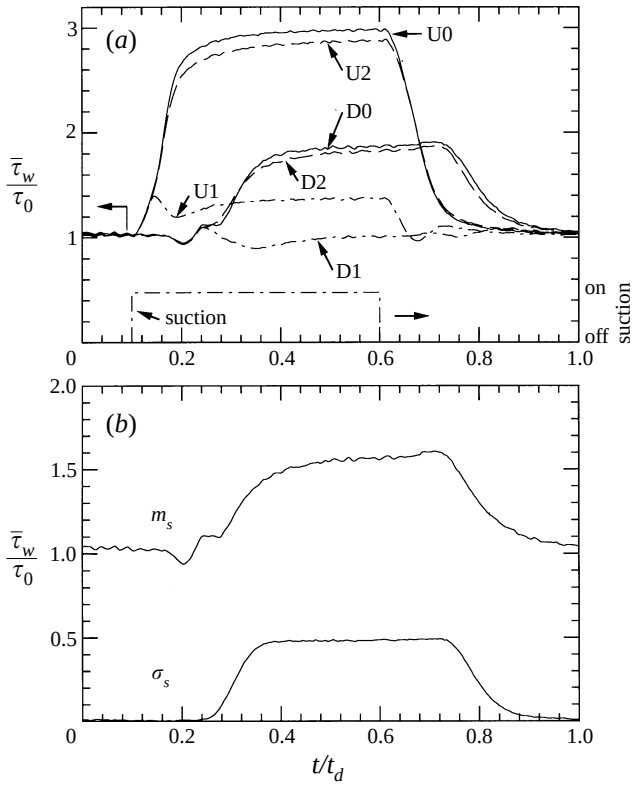

FIGURE 19. Pulsed suction disturbance with no actuation, phase-averaged results: (*a*) individual sensor measurements and suction disturbance timing; (*b*) m_s and σ_s.

passing disturbance, with sensors D0 and D2 showing an increase in shear and sensor D1 a slight decrease. Although the disturbance weakened as it was convected downstream, it was still substantial when it passed over the downstream sensors.

Figure 19(*b*) shows the mean (m_s) and standard deviation (σ_s) of the three downstream shear measurements shown in figure 19(*a*). These parameters provide a measure of the spanwise-integrated wall shear and the spanwise uniformity of the wall shear in the region of the downstream sensors. The control objective was to attenuate the unsteady suction disturbance of figure 19, as measured by m_s and σ_s.

4.3. *Feedforward/feedback control*

If the amplitude of a fluid disturbance were relatively constant as it passed over a control module (as was true for the disturbances used here), then a possible control algorithm would be an optimization routine searching for actuator amplitudes that minimized a performance index formed from m_s and σ_s. This scheme was attempted, and was unsurprisingly successful, with one caveat. The controller needed about five update steps before starting to converge around the minimum. However, the period of each update step was constrained to be larger than the convective time lag from a change in amplitude of the actuators until this change was observable at the downstream sensors. The five update step convergence time for this controller was on the order of the expected lifetime of streaky structures in the turbulent boundary layer section of the flow tunnel. Thus control optimization during the passage of a finite time disturbance did not seem feasible.

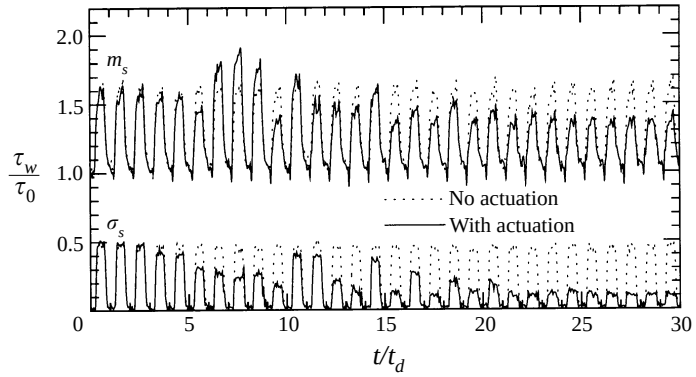

FIGURE 20. Periodic pulsed suction disturbance with fast feedforward/slow feedback control to minimize the performance index. Instantaneous values of m_s and σ_s are shown.

One way to alleviate this problem might be to reduce the distance between the actuators and downstream sensors. However, as will be shown later in this section, this can result in sensor measurements that are inconsistent with the ultimate control effect of the actuators. The actuators generate a v disturbance that transports fluid to produce a u disturbance. It is the u disturbance that is detectable by the sensors. This process takes time, and in a convection-dominated system, time is equivalent to downstream distance.

A control strategy was chosen which removed the above concern. The upstream sensors were unencumbered by any type of convective time lag. A predetermined controller specified actuator amplitudes based on the upstream sensor measurements, with an appropriate time lag to account for the convection time from the upstream sensors to the actuators. This convection time was determined by measuring the passage time of a disturbance from the upstream to downstream sensors, corrected by a geometric factor accounting for the location of the actuator between the sensors. This process is an example of *feedforward* control, and can occur at a sample and update rate that is large compared to disturbance frequencies.

The downstream sensors were also sampled at the same frequency as the feedforward control system. The data collected from the downstream sensors during the complete passage of a disturbance were combined to form a performance measure of the actuator control on the disturbance. An optimization algorithm used the performance measure to modify the controller. In this way, the controller was modified once after the passage of each disturbance. This process is an example of *feedback* control. The feedback operated at the disturbance frequency, which was relatively slower than the rate at which feedforward information was used.

The combined feedforward and feedback control procedure is referred to here as fast feedforward/slow feedback control. This process is illustrated in the top portion of figure 17.

Figure 20 shows an example of a typical control result using this procedure. The suction disturbance period, t_d, was 4 s (consistent with the disturbance of figure 19). Each cycle visible in figure 20 is the passing of a suction disturbance. The upstream and downstream sensors were sampled and the actuator amplitudes were updated at 50 Hz. The disturbance identification criterion was based on the difference between the measurements from sensor U1 and sensors U0 and U3. When (U0–U1) and (U3–U1) were greater than a set value for several consecutive measurements, a disturbance

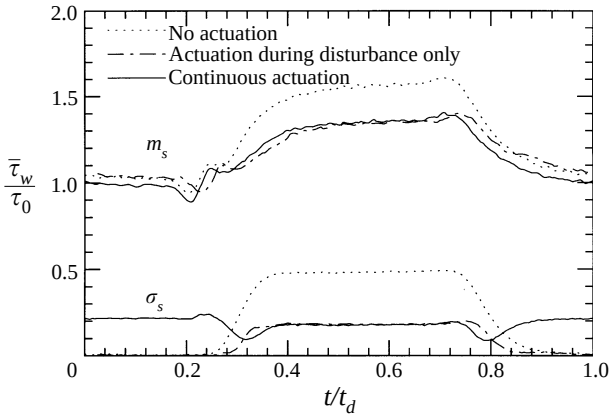

FIGURE 21. Pulsed suction disturbance with continuous actuation compared to cases with no actuation and with actuation only during the disturbance passage, phase-averaged results.

was considered identified. When the criterion was no longer satisfied, the disturbance was considered passed. The downstream sensor data taken when the disturbance was overhead were averaged over the disturbance lifetime, and passed to the controller.

The downstream sensor data, m_s and σ_s^2, were linearly combined to form a performance index. For this example, the controller was an algorithm that attempted to minimize the performance index averaged over a disturbance. The downhill simplex method of Nelder & Mead (1965) (also Press *et al.* 1992) was used for the minimization algorithm. This method is attractive in that it uses only functional evaluations, and requires no gradient information. The controller specified a set of actuator amplitudes that became associated with a performance index after the passage of a disturbance. This value of the performance index was then used by the optimization algorithm to generate a new set of actuator amplitudes to try on the next disturbance.

The controller was initiated to start its search with zero actuator amplitudes (i.e. no control). By the end of the run, the peak of m_s was decreased by 10% and the peak of σ_s was decreased by about 80%. The minimization algorithm found a good set of controls by the tenth disturbance, but it was only after about twenty disturbances that the algorithm settled upon the minimum.

The control algorithm did not depend on the periodicity of the disturbance. Control runs were performed with aperiodic disturbances, and results comparable to those shown in figure 20 were obtained.

It was assumed that the control actuators should be used only while the suction disturbance was passing over the actuators. This assumption is confirmed in figure 21, which shows phase-averaged results for an experiment in which the control actuators were always on. Results for a case with no actuation and for a case with actuation using the controller determined in the run of figure 20 are also shown. Although the reduction in m_s and σ_s is obtained during the suction disturbance for both actuation cases, the continuous actuation case caused a significant increase in the wall shear spanwise variation when it was not counteracting the suction disturbance.

4.3.1. *Mean velocity measurements*

The interaction of the actuator disturbance with the suction disturbance was investigated using mean velocity measurements. The suction disturbance was held

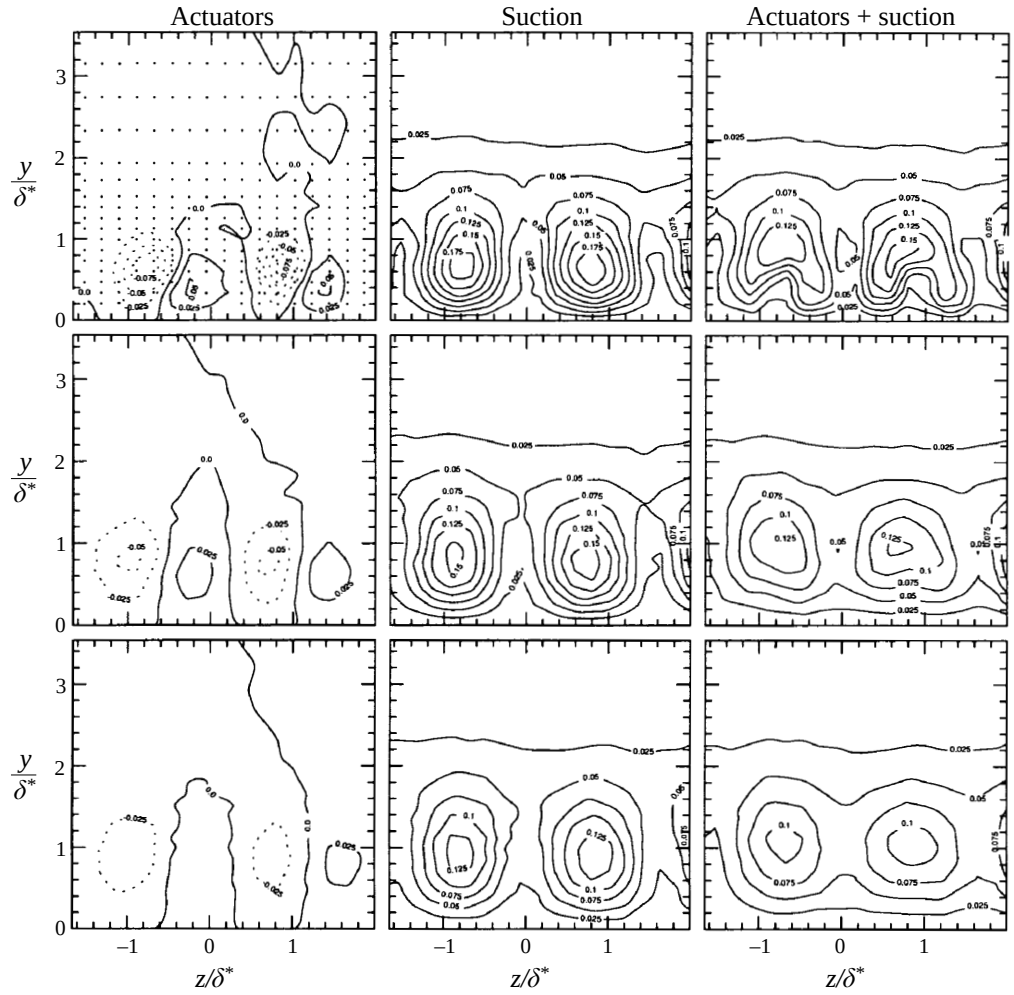

FIGURE 22. Steady suction disturbance control: streamwise velocity disturbance ($\Delta U/U_\infty$) contours for runs with the actuator alone, suction alone, and combined actuator/suction at $\Delta x/\delta^* = 5$ (top row), 17 (middle row), 29 (bottom row).

steady. The actuator amplitudes were set to values found during the suction disturbance by the controller of the previous section. Figure 22 shows contour plots of the U disturbance resulting from the actuator alone, the suction disturbance alone, and the control of the suction disturbance with actuation. The columns of figure 22 show results for each type of disturbance, and the rows show results at different downstream locations. Positive contours are shown as solid lines and negative contours as dashed lines. The measurement grid is shown superimposed on one of the plots. The measurements focused on the central common-flow-up vortex pair disturbance from the suction which creates a central low-speed streak surrounded by high-speed streaks. This structure is clear in the central column of figure 22.

The results at $\Delta x/\delta^* = 5$, the location of the downstream wall shear sensors, show data consistent with the control results of figure 20. In the combined actuator/suction run, the nearest wall contour line was pushed away from the wall in the regions

$\Delta x/\delta^*$	% reduction in $(\Delta U)^2$ area integral	% reduction in near-wall U spanwise-averaged mean	% reduction in near-wall U spanwise-averaged standard deviation
0.5		3%	−11%
5	18%	2%	21%
17	20%	4%	41%
29	19%	3%	26%

TABLE 1. Reductions in the suction disturbance by actuator-control with respect to the suction disturbance with no control.

of highest shear, and was pulled towards the wall in the region of lowest shear, thus reducing the near-wall spanwise variations in U. In addition, the actuation weakened the peak strength of the high-speed streak and strengthened the low-speed streak. This effect continues in the downstream measurements, where the reduction in strength of the high-speed streaks is clear. To quantify this effect, the square of the U disturbance was integrated over the range $0 < y/\delta^* < 2.2$ and $-1.6 < z/\delta^* < 1.6$, the approximate area over which the controlled portion of the suction disturbance extends. The results are summarized in table 1, which shows a consistent $\approx 20\%$ reduction at all stations when the actuator-controlled suction disturbance was compared to the suction disturbance alone.

Finer resolution spanwise profiles of the streamwise velocity were taken at $y/\delta^* = 0.25$, at the same streamwise locations as the contour data of figures 22, with an additional profile at $\Delta x/\delta^* = 0.5$. At this distance from the wall, the streamwise velocity trends are comparable to the streamwise wall shear trends. The mean and standard deviation of these velocity profiles were calculated, and the reductions in these values, when comparing the actuation case to the no-actuation case, are summarized in table 1. There was a significant reduction in the standard deviation, peaking at 41% at $\Delta x/\delta^* = 17$. However, the reduction in the mean was only a few percent at each measurement station. The reductions in the mean and standard deviation of the spanwise velocity profile at $\Delta x/\delta^* = 5$, the location of the downstream sensors, were not nearly as large as those measured by the sensors, which showed an 11% reduction in the spanwise mean and a 66% reduction in the standard deviation for this run. This indicates that the sensors, although indicative of the trends in the flow, did not fully resolve the flow. The velocity measurements did resolve the flow, and the results in table 1 are considered valid measures of the control effects on the suction disturbance.

The results in table 1 at $\Delta x/\delta^* = 0.5$ show that the effects of the control were measurable close to the actuator tip, although the spanwise profile here showed an increase in standard deviation compared to the uncontrolled case. It must be kept in mind that the actuator disturbance occurs along the length of the narrow side gap, although it is strongest at the downstream end. Since the actuator disturbance starts upstream of the actuator tip, it is not unreasonable that a control effect was measurable close to the tip. But the effect measurable at the actuator tip was not consistent with the trends shown further downstream, in terms of the reduction in spanwise variations. Further downstream the control disturbance has had a longer time to interact with the flow disturbance, and this is clearly significant.

Thus, the results in table 1 indicate that the downstream sensors could have

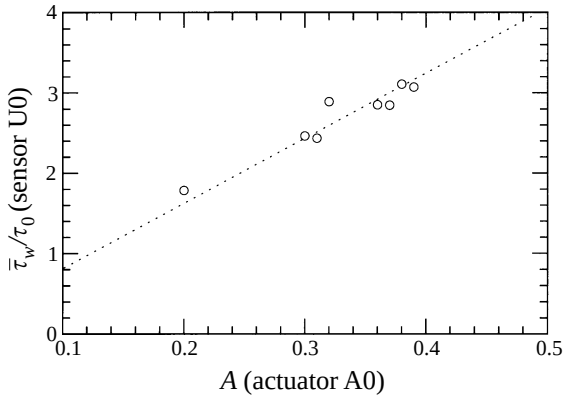

FIGURE 23. Optimal actuator amplitude as a function of the measurement from an upstream sensor. Suction strength was varied by changing the suction rate.

been moved somewhat closer to the actuator tips, reducing the convective time lag. However, there was a limit as to how close they could have been moved before their utility for control was compromised.

4.3.2. *Disturbance variations*

For all of the control runs presented, the suction disturbance strength was kept constant. This simplified the problem, making the control a simple minimization. However, natural flow disturbances are likely to have varying and time-dependent strength. The fast feedforward/slow feedback control concept is equally applicable to variable-strength disturbances. The simple minimization model used above would be replaced with a parametric model or schedule for the controller that could provide different actuator strengths based on the measured upstream disturbance. The slow feedback technique could then be used to adapt the model parameters as flow conditions change. As a test of this concept, the suction rate was varied, and the control algorithm found the optimal actuator amplitude associated with the new suction rate. Figure 23 shows a plot of the shear measured by sensor U0, a measure of the disturbance strength, versus the optimal amplitude for actuator A0 found by the minimization algorithm. The relationship is nearly linear, and a simple control model could be constructed based upon this data.

5. Conclusions

A new type of vortex generator has been developed for use as an actuator for boundary layer control experiments. The actuator, using piezoelectric forcing, produces a pair of quasi-steady streamwise vortices, with common-flow away from the wall, in the near-wall region of the boundary layer. The vortices are localized over the actuator, and decay rapidly downstream within a few displacement thicknesses. However, the generated low-speed streak persists much farther downstream. The actuator described in this paper was demonstrated in a laminar boundary layer using water. The actuator has also been demonstrated in air (Saddoughi 1994, 1995; Saddoughi *et al.* 1997) and in a turbulent boundary layer (JR). The actuator has several desirable features in terms of its use for near-wall boundary layer control:

On-Demand: the actuator is flush mounted with the boundary surface so it disturbs the flow only when it is turned on.

Controllable: the disturbance to the flow from the actuator is a function of the drive amplitude.

Zero Net Mass Addition: the actuator does not require a fluid source.

Compact: the actuator design should lend itself nicely to fabrication in large arrays of small-scale sensors and actuators using planar microelectromechanical systems (MEMS) technology. Considerable development of MEMS technology is necessary, however, particularly in terms of lifetime and robustness, before its use will be feasible for practical engineering control situations.

Fast: the rise time of the actuator cantilever is a few cycles of the drive frequency. The actuator can be designed so that its resonance frequency is significantly higher than the frequency of the events one seeks to control in the flow.

The actuator was used to interact with disturbances generated by a cylinder placed normal to the flow. Despite a mismatch in scale between the cylinder-generated disturbance and the actuator control disturbance, the actuator was still able to push the laminar–turbulent transition, caused by the cylinder disturbance, downstream by about 40 displacement thicknesses. The greatest transition delay was obtained when the actuator was approximately aligned with one of the inflection points in the spanwise profile of the cylinder disturbance rather than with the centre of the cylinder disturbance. These results suggest that an actuator that generates structures over a limited range of scales can still be useful for control of disturbances over a wider range of scales. This has broad implications for control in a turbulent flow where a wide range of scales can be expected.

The actuator was also used to interact with unsteady low- and high-speed streaks generated by pulsed suction. A control module consisting of a transverse actuator array along with upstream and downstream arrays of sensors was fabricated. A strategy for controlling unsteady convecting disturbances was developed using fast feedforward of upstream sensor information to detect disturbances and slow feedback of the downstream controlled disturbance to adapt the controller. An implementation of this fast feedforward/slow feedback strategy resulted in a substantial decrease in the spanwise variation of an unsteady disturbance as measured at the sensors downstream of the actuators.

The actuators were situated to speed up the low-speed streaks and slow down the high-speed streaks. The control did a good job in reducing the spanwise gradients of the streamwise velocity, which was one of the goals. Swearingen & Blackwelder (1987) showed that the instability associated with inflectional spanwise profiles of the streamwise velocity, formed by streamwise vortices, was an important feature in the breakdown of near-wall vortices. This suggests that a control that smooths out spanwise profiles has the potential to disrupt the bursting cycle observed in turbulent boundary layers.

However, the control in §4 only marginally decreased the mean of the spanwise profile of the streamwise velocity. In speeding up the low-speed flow and slowing down the high-speed flow, on average, the control reduced the mean of the spanwise profile by only a few percent. This small effect on the spanwise profile mean is likely due to the relatively linear nature of a laminar boundary layer near the wall.

We believe the fast feedforward/slow feedback control scheme presented in this paper is generally applicable to control of fully turbulent flows. However, a fully turbulent flow presents several additional difficulties over those encountered in this paper. Sensing will be much more difficult, and there is a need for improved streak detection algorithms to work within the control scheme. Rathnasingham & Breuer (1997) have performed some recent work towards this end. A turbulent flow will

also present smaller scales and higher frequencies. We believe that microfabrication of actuator and sensor arrays will satisfy the length scale requirements and proper design of the cantilever stiffness will satisfy the frequency response requirements. However, if net drag reduction is the goal, the power consumption of the actuators and sensors must be reduced.

In addition to the control scheme described in this paper, adaptive neural-network based controllers were also implemented on the pulsed suction disturbance control problem of § 4. The control results were similar to those described here. The neural network control results are discussed in JR.

This work was prepared with the support of the AFOSR under contract AFOSR-91-0072, Dr James McMichael, program manager. S.A.J was also supported in part by a National Science Foundation graduate fellowship. The authors wish to thank Professor Ari Glezer of Georgia Tech for introducing them to piezoelectric cantilever actuators. The authors also wish to thank Professor Kenneth Breuer of MIT for several useful discussions.

REFERENCES

Acarlar, M. S. & Smith, C. R. 1987 A study of hairpin vortices in a laminar boundary layer. Part 2. Hairpin vortices generated by fluid injection. *J. Fluid Mech.* **175**, 43–83.

Blackwelder, R. F. & Eckelmann, H. 1978 The spanwise structure of the bursting phenomenon. In *Structure and Mechanisms of Turbulence* (ed. H. Fiedler), vol. 1, p. 190. Springer.

Blackwelder, R. F. & Haritonidis, J. H. 1983 Scaling of the bursting frequency in turbulent layers. *J. Fluid Mech.* **132**, 87–103.

Blackwelder, R. F. & Liu, D. 1994 Delay of break-down of streamwise vortices embedded in a boundary layer. In *Turbulence Control* (ed. D. E. Parekh). FED-Vol. 193, pp. 9–18. ASME.

Breuer, K. S. & Haritonidis, J. H. 1990 The evolution of a localized disturbance in a laminar boundary layer. Part 1. Weak disturbances. *J. Fluid Mech.* **220**, 569–594.

Breuer, K. S., Haritonidis, J. H. & Landahl, M. T. 1989 The control of transient disturbances in a flat plate boundary layer through active wall motion. *Phys. Fluids* A **1**, 574–582.

Breuer, K. S. & Kuraishi, T. 1993 Bypass transition in two- and three-dimensional boundary layers. *AIAA Paper* 93-3050.

Breuer, K. S. & Landahl, M. T. 1990 The evolution of a localized disturbance in a laminar boundary layer. Part 2. Strong disturbances. *J. Fluid Mech.* **220**, 595–621.

Bushnell, D. M. & McGinley, C. B. 1989 Turbulence control in wall flows. *Ann. Rev. Fluid Mech.* **21**, 1–20.

Fiedler, H. E. & Fernholz, H. H. 1990 On management and control of turbulent shear flows. *Prog. Aerospace Sci.* **27**, 305–387.

Gad-el-Hak, M. 1996 Modern developments in flow control. *Appl. Mech. Rev.* **49**, 365–379.

Gad-el-Hak, M. & Blackwelder, R. F. 1987 Control of the discrete vortices from a Delta wing. *AIAA J.* **25**, 1042–1049.

Gad-el-Hak, M. & Hussain, A. 1986 Coherent structures in a turbulent boundary layer. Part 1: Generation of "artificial" bursts. *Phys. Fluids* **29**, 2124–2139.

Gedney, C. J. 1983 The cancellation of a sound-excited Tollmien-Schlichting wave with plate vibration. *Phys. Fluids* **26**, 1158–1160.

Jacobson, S. A. & Reynolds, W. C. 1993 Active boundary layer control using flush-mounted surface actuators. *Bull. Am. Phys. Soc.* **38**, 2197.

Jacobson, S. A. & Reynolds, W. C. 1995 An experimental investigation towards the active control of turbulent boundary layers. *Stanford University Thermosciences Division Rep.* TF-64 (referred to herein as JR).

Kline, S. J., Reynolds, W. C., Schraub, F. A. & Runstadler, P. W. 1967 The structure of turbulent boundary layers. *J. Fluid Mech.* **30**, 741–773.

KOUMOUTSAKOS, P. 1995 Simulations of vortex generators. *Center for Turbulence Research, Annual Research Briefs*, pp. 233–240.

LIEPMANN, H. W., BROWN, G. L. & NOSENCHUCK, D. M. 1982 Control of laminar-instability waves using a new technique. *J. Fluid Mech.* **118**, 187–200.

MILLING, R. W. 1981 Tollmien-Schlichting wave cancellation. *Phys. Fluids* **24**, 979–981.

MOIN, P. & BEWLEY, T. 1994 Feedback control of turbulence. *Appl. Mech. Rev.* **47**, S3–S13.

NELDER, J. A. & MEAD, R. 1965 A simplex method for function minimization. *Computer J.* **7**, 308–313.

ORLANDI, P. & JIMÉNEZ, J. 1994 On the generation of turbulent wall friction. *Phys. Fluids* **6**, 634–641.

PRESS, W. H., TEUKOLSKY, S. A., VETTERLING, W. T. & FLANNERY, B. P. 1992 *Numerical Recipes in Fortran*. Cambridge University Press.

RATHNASINGHAM, R. & BREUER, K. S. 1997 System identification and control of a turbulent boundary layer. *Phys. Fluids* **9**, 1867–1869.

SADDOUGHI, S. G. 1994 Experimental investigations of "on-demand" vortex generators. *Center for Turbulence Research, Annual Research Briefs*, pp. 197–203.

SADDOUGHI, S. G. 1995 Preliminary results of the "on-demand" vortex generator experiments. *Center for Turbulence Research, Annual Research Briefs*, pp. 227–232.

SADDOUGHI, S. G., KOUMOUTSAKOS, P., BRADSHAW, P. & MANSOUR, N. N. 1997 Preliminary experimental and numerical investigations of "on-demand" vortex generators. *Phys. Fluids* (submitted).

SCHILZ, W. 1965/66 Experimentelle untersuchungen zur akustischen beeinflussung der stromungs-grenzschicht in luft. *Acustica* **16**, 208–223.

SWEARINGEN, J. D. & BLACKWELDER, R. F. 1987 The growth and breakdown of streamwise vortices in the presence of a wall. *J. Fluid Mech.* **182**, 255–290.

THOMAS, A. S. W. 1983 The control of boundary-layer transition using a wave-superposition principle. *J. Fluid Mech.* **137**, 233–250.

VAN DYKE, M. 1982 *An Album of Fluid Motion.* The Parabolic Press.

WILTSE, J. M. & GLEZER, A. 1993 Manipulation of free shear flows using piezoelectric actuators. *J. Fluid Mech.* **249**, 261–285.